Politecnico
di Torino

MASTER'S THESIS

Submitted to

Politecnico di Torino

Automotive Engineering

MASTER DEGREE IN AUTOMOTIVE ENGINEERING

By

Pietro Ronzio

THERMAL MODEL OF LI-ION BATTERY BASED ON A SINGLE TEMPERATURE LUMPED PARAMETER MODEL

Ms. Daniela Anna Misul — Supervisor

July 2022

Author's Declaration of Originality

I hereby certify that I am the sole author of this thesis. All the used materials, references to the literature and the work of others have been referred to. This thesis has not been presented for examination anywhere else.

Author: Pietro Ronzio

06-07-2022

Dedication

Alla nonna.

Acknowledgments

I would like to thank Prof.ssa Daniela Anna Misul that gave me the possibility to work on this thesis topic in such a difficult situation due to COVID emergency when there weren't any interesting proposals from other companies or professors.

A special thanks also to the two PhD students, Alessandro Falai and Tiziano Giuliacci, that followed me in the development of this topic and helped me every time I was stuck or I needed some suggestions on how to proceed.

Abstract

In recent years, electrification of transportation sector has become more relevant due to the growing necessity to reduce pollutants emitted by conventional engines, fed with carbon fossil fuels. One of the most important components of an electric powertrain is the energy storage system, usually a Lithium Ion battery, responsible of energy storage and generation of electric current to make the motor work. Among different factors affecting battery characteristics, such as performances, life time and safety, temperature is the one of biggest impact; thus its influence during normal working conditions must be monitored and studied. This thesis introduces a thermal lumped parameter model of a battery, implemented in MathWorks Matlab R2021a environment, able to estimate its temperature while undergoing some reference test cycles. Firstly, an equivalent circuit model with two RC branches of a single cell has been developed in order to simulate its behaviour. To assess the dependency of circuit parameters on temperature, a procedure of parameters identification has been carried out, where at each iteration, every parameter has been updated in order to match the simulated battery tension with the experimental data coming from the literature. Then, a thermal model has been developed following the classical energy balance equation and Bernardi's equation of heat generation whose fundamental parameters, as convective heat transfer coefficient and specific heat, have been calibrated. Obtained results suggest that parameter identification procedure has correctly reported temperature influence on battery parameters, as well as considering the entropic term in the heat generation has helped in lowering the two thermal coefficients, assuming more realistic values. Finally a battery model made out of 25 cells has been constructed in the Simscape environment, whose results have been shown compatible with expectations, although the lack of a validation procedure with experimental data.

List of Abbreviations and Terms

Abbreviations

BMS	Battery Management System
CFD	Computational Fluid Dynamics
ECM	Equivalent Circuit Model
ECU	Electronic Control Unit
ESS	Energy Storage System
EV	Electric Vehicle
HEV	Hybrid Electric Vehicle
HPPC	Hybrid Pulse Power Characterization
ICE	Internal Combustion Engine
LCO	Lithium Cobalt Oxyde
LFP	Lithium Iron Phospate
LMO	Lithium Manganese Oxyde
NCA	Nichel Cobalt Aluminum
NMC	Nichel Manganese Cobalt
OCV	Open Circuit Voltage
OEM	Original Equipment Manufacturer
OOL	Optimum Operating Line
PHEV	Plugin Hybrid Electric Vehicle
SEI	Surface Electrolyte Interface
SOC	State Of Charge
SOH	State Of Health

Nomenclature

c	Capacitance Rate
c_p	Specific Heat
C	Capacitance
D	Diameter of the Cylinder
g	Acceleration due to gravity
h	Air Heat Transfer Coefficient
H	Hessian Matrix

I	Current
k	Thermal Conductivity
Nu_D	Nusselt Number
Pr	Prandtl Number
q	Heat
R	Resistance
Ra_D	Rayleigh Number
s	Layer Thickness
S_h	Volumetric Source Term
T_b	Battery Temperature
V	Tension
V_{OCV}	Open Circuit Voltage
V_{out}	Battery Output Voltage
α	Thermal Diffusivity
β	Thermal Expansion Coefficient
ϵ	Emissivity
λ	Material Thermal Conductivity
σ	Stefan Boltzmann Constant
τ	Time Constant
θ	Kinematic Viscosity

Table of Contents

List of Figures

List of Tables

General Introduction

The aim of this thesis is to present a thermal lumped parameter model of a battery to estimate its working temperature while functioning.
To do so, it is necessary to study electrical, chemical and thermal properties of a battery, how they can be modelled and in which way their interaction affects its overall performances.

Nowadays, in a society like ours, where population keeps increasing and so the economy does, the demand of vehicles is rising in all the fields, from public to private and commercial transportation.
Unfortunately, also the atmospheric pollution due to the combustion products coming from internal combustion engines (ICE), such as carbon monoxide (CO) and dioxide (CO2), nytrogen oxydes (NOx) and unburnt hydrocarbons (HC), keeps growing in a dangerous way for the health of the planet and, as consequence, also for the health of the billion of people who are living on it.

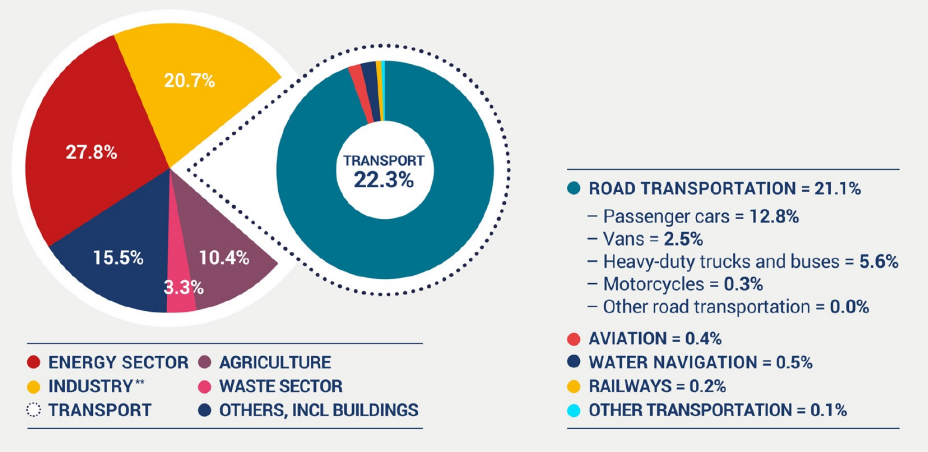

Figure 1. CO2 Emissions

To recover from this situation, many nations from all around the world have decided, among other things, to limit the emissions directly related to vehicles, thus arriving to the conclusion that electrification of the transportation sector is mandatory.
A part from the pollution issues, electrification can be also seen as an opportunity to improve the centenary ICE technology for what concerns their performances.
This concept is usually referred to as "hybridization", different from full electrification, and it has already been adopted also in race competition as Formula 1.

Main advantages of hybridization, depending on its architecture, are the possibility to make the ICE working on the so called OOL "Optimum Operating Line", i.e. the line of maximum efficiency points for each power level, thus leading to lower emissions, as well as boosting the performances of an engine when it is required, for instance during a sudden acceleration phase.
Regarding the latter application, Lamborghini has had the idea to replace the Lithium Ion battery with Supercapacitors, a special kind of electric energy storage system, as primary source of electric power, thus giving stunning acceleration capabilities to their highest end prototype car, the Lamborghini Terzo Millennio.
Anyway, since performances of the batteries are strongly related to their working temperature, it is important to study and to understand their thermal behaviour in order to design proper battery management system (BMS) and cooling strategies also to assure the maximum safety.

Figure 2. Lamborghini Terzo Millennio endowed with Supercapacitors

To arrive to the development of a battery model made by an assembly of different cells in series or parallel, it is first necessary to develop a model for a single cell.
First of all, an electric circuit of the cell representing its electro-chemical characteristics is required to simulate its performances under defined working loads: between different kind of models, the equivalent circuit model (ECM) with two RC branches has been chosen as the best one in terms of computation time and accuracy.
This has been done by employing Simulink environment to solve the electrical equations of the equivalent circuit of the battery as it will be explained in the apposite section of the chapter 1.
Then, once the ECM has been made, a procedure of parameter optimization has been

carried out in order to assess the ECM parameters dependency on temperature and state of charge (SOC). The results coming from this procedure has been obtained by comparing modelled signal with experimental signal provided by the literature [1].
Finally, the thermal model of the single cell can be implemented to estimate its temperature, by solving the first order differential equation of energy balance, always employing Simulink.
After the calibration process of the single cell model, especially for what concerns the convective heat transfer coefficient and specific heat of the battery, a simplified battery model has been developed.
This time, it has been chosen to employ Simscape environment due to its easier and faster implementation with respect to the Simulink one for this kind of works.

In the first chapter of this thesis, the state of art of battery has been investigated; in particular the one regarding Lithium Ion batteries has been explored in depth.
The second chapter focuses on the single cell model and its validation with literature data.
A simplified battery model composed of 25 cells has been developed and analysed in the third chapter.

1. State of the Art

In the first section of this chapter, a description of different kinds of batteries and the general working principle have been presented, with their characteristics and performance parameters, in order to assess which are the most useful and employed in the automotive field, according to the required task.

It follows a second section where lithium batteries have been explored more in depth, in particular their structure, chemistry and what kind of failures they can encounter during their life.

Theoretical electrical and thermal models to predict the behaviour of batteries have been presented in the final section of this chapter, where the physics and equations behind these models have been explained, highlighting principal advantages and disadvantages of each model.

1.1 Electrochemical Cells

Electrochemical cells can be divided into three categories: batteries, capacitors, and fuel cells.
Capacitors are elements able to provide high amount of energy for short period of time, while fuel cells are able to produce electric energy from the reaction of hydrolysis occurring between oxygen and hydrogen; not involving fossil fuels, the only product from this reaction is water.
However, since this thesis is focused on the analysis of a battery pack, the other two will not be considered throughout this dissertation.
Batteries are electrochemical energy storage devices able to convert the chemical energy contained in their active material directly into electric energy.
The conversion process occurs throughout an electrochemical oxidation-reduction (redox) reaction, i.e. transferal of electrons from the electrode suffering oxidation to the one being reduced.

$$Reduction \;\; \mathrm{A}^{n+} + \mathrm{ne}^{-} \longrightarrow \mathrm{A}$$

$$Oxidation \;\; \mathrm{A}^{n-} \longrightarrow \mathrm{A} + \mathrm{ne}^{-}$$

These reactions can be both one directional ("primary" batteries only for discharge) or reversible, as in the so called "secondary" batteries that can be recharged, for instance to

implement the regenerative breaking on hybrid vehicles (Fig. 3).
The particularity in batteries is that these redox reactions take place in separate places inside the battery, forcing the electrons to travel from one electrode to the other.
If the load to be powered is located in the electrical path the electrons are moving through, then power can be used to generate work [2].
Electrochemical cells, as shown in Fig.4 are made of :

- anode electrode where oxidation reduction takes place.
- cathode electrode where reduction reaction takes place.
- separator, porous membrane between the two electrodes to insulate them each other, making pass only positive ions.
- electrolyte (liquid, gel or solid) acting as carrier for ion flow between the electrodes.
- current collectors (one positive and one negative) to connect the cell to other cells or to the electric source/load.

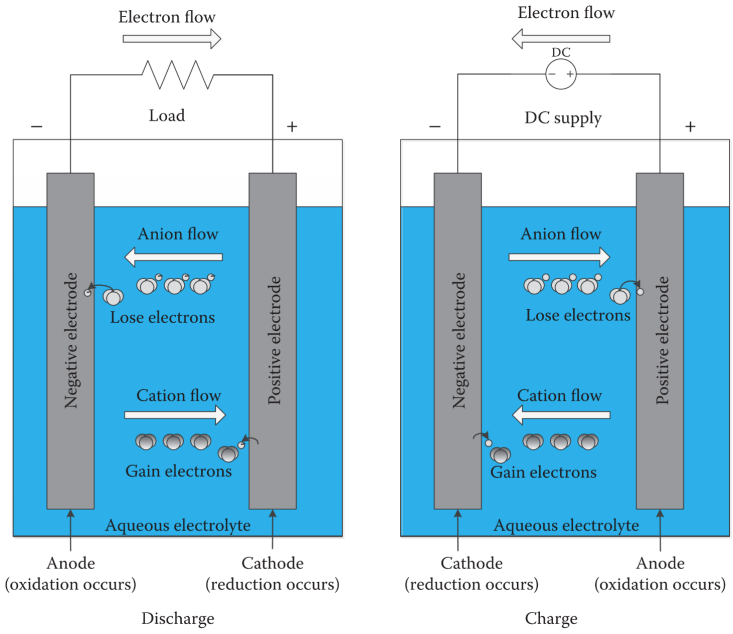

Figure 3. Discharge and charge phases (Adapted from Linden, D., and T.B.Reddy.Handbook of Batteries. New York, 2002.)

1.1.1 Battery Cell Requirements

With hybrid electric vehicles (HEVs), plug-in hybrid electric vehicles (PHEVs), and electric-only vehicles (EVs) approaching the point of entering the market in mass-production volumes, the search has intensified for advanced energy storage technologies that offer the energy storage system (ESS) with increased energy density, power density, durability, safety, and affordability [2].
Among these, the two most important factors affecting battery perfomance and their choice

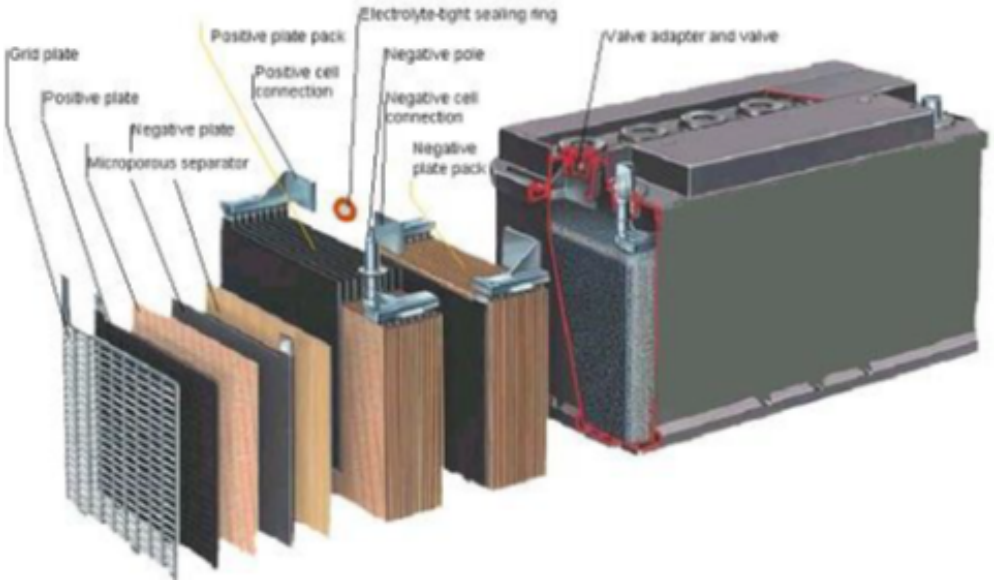

Figure 4. 12V lead battery module (automotive auxiliary battery)

according to their task, are the specific power and the specific energy, respectively the amount of power each kilogram of battery can deliver and the amount of energy stored per unit mass.

In particular the specific power is required to satisfy limited time requests at high power demand, when, for instance, a boost for rapid acceleration is necessary, while specific energy is required to satisfy long duration tasks at lower-mid power demand, i.e. to maximize the range of an EV.

The latter is also the main responsible of weight, volume and cost of the energy storage system.

Unfortunately one the main issues of the batteries is the practical impossibility to design the cells to have at the same time both the highest specific power and the highest specific energy.

As a consequence, usually the battery sizing is the outcome of a compromise.

A useful tool to compare perfomances of different kind of batteries is the so called "Ragone Plot" (Fig.5), a graph showing for each kind of batteries, its specific power and specific energy.

Finally table 1 highlights the characteristic of commonly used type of batteries: Lead acid, Nichel Metal Hydride, Lithium ion, Sodium Nichel Cloride.

Lead acid type is very common, expecially for automotive starting, lighting and to feed current for the spark ignition. Anyway its implementation is not suitable for traction purposes due to its limited specific energy.

Nichel Metal Hydride are implemented only for power buffer applications because of their limited operational delta SOC, meaning they cannot be fully charged or discharged, otherwise they would be damaged.

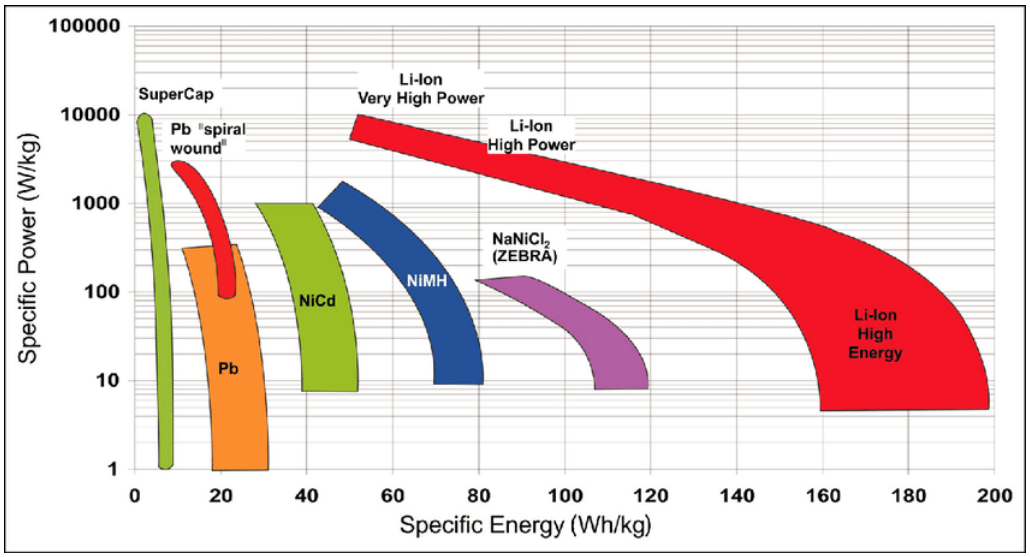

Figure 5. Ragone Plot - Specific Power vs Specific Energy

Sodium Nichel Cloride batteries are also called "hot batteries" since they reach high temperatures while functioning at about 270°C.
Due to their good specific energy, they are usually implemented for traction.
In conclusion, Lithium ion batteries are nowadyas the most promising in terms of specific energy and density, reaching a good compromise between added weight to the vehicle and perfomances. However their cost is strongly impacting on the overall cost of an electric vehicle.
It is worth to mention the stunning performances of ultra capacitors for what concerns their specific power: being so high, they are use for power buffer applications, as happens on the Lamborghini Terzo Millennio.

	Lead Acid	NiMH	Li-ion	Na-Ni-Cl
Specif energy (Wh/kg)	30-50	60-120	120-265	100-120
Energy density (Wh/L)	50-80	140-300	250-730	150-180
Specif power (W/kg)	75-300	250-1000	250-340	150-200
Power density (W/L)	10-400	80-300	100-210	220-300
Round-trip efficiency (%)	70-80	60-70	85-98	85-90
Self discharge (%/day)	0.033-0.3	25-30	0.1-0.3	15
Cycle lifetime (cycles)	100-2000	500-1000	400-1200	2500
Power capacity cost ($/kW)	175-600	150-1500	175-4000	150-300
Energy capacity cost ($/kWh)	150-400	150-1500	500-2500	100-200

Table 1. Comparison of Electrical Energy Storage Technologies (Source: Augmented from Bradbury, K. Energy Storage Technology Review. Duke University, Durham, NC, 2010: 1–34.)

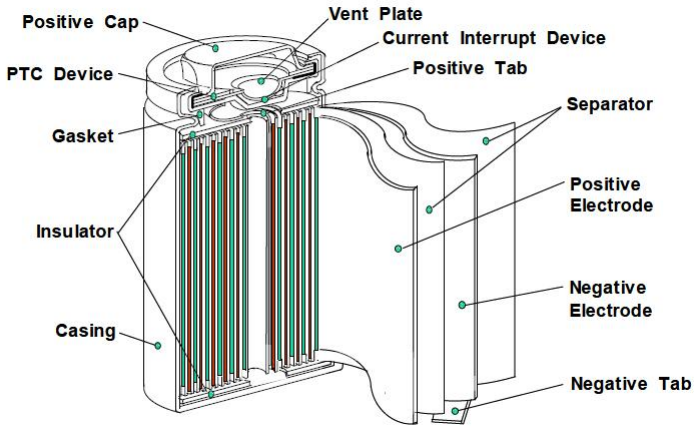

Figure 6. Cylindrical Cell

1.2 Lithium Ion Cells

Todays batteries for EV are made of Lithium Ion cells for the majority of vehicles due to their capabity to reach a good trade off between weight, perfomances, and cost that customers can afford.
Furthermore, the technology is always improving and while it is getting more efficient both in term of production and perfomance, also its price is decreasing since the offer from various OEM is growing and competition among them helps in lowering it.

1.2.1 Lithium Ion Main Typologies

The first classification of Li-Ion cells concerns their package.
There are three main types: cylindrical, prismatic and pouch cells.
Cylindrical cells (Fig.6) have a metallic container which gives an high robustness and a good cooling capability, but they are heavier and bigger thus reducing the available space for other cells.
Prismatic cells (Fig.7) have an aluminum or metal case, providing high robustness and at the same time a simpler geometry which allows a better overall packaging, occupying less space. Furthermore a better thermal dissipation can be achieved with respect cylindrical cells.
Pouch typology (Fig.7) are typical of lithium polymer cells. This structure allows more flexibility and lowers the weight of the cell, anyway it requires an additional case because of this high flexibility. They also show a good thermal dissipation and they are cheaper than other types of cells. For this reason they are widely spread on the market. The major drawback is that they blow up if misused.
The second classification regards the chemistry of the cathode active material of the cells whose characteristics for what concerns efficiency, perfomances, durability and safety are

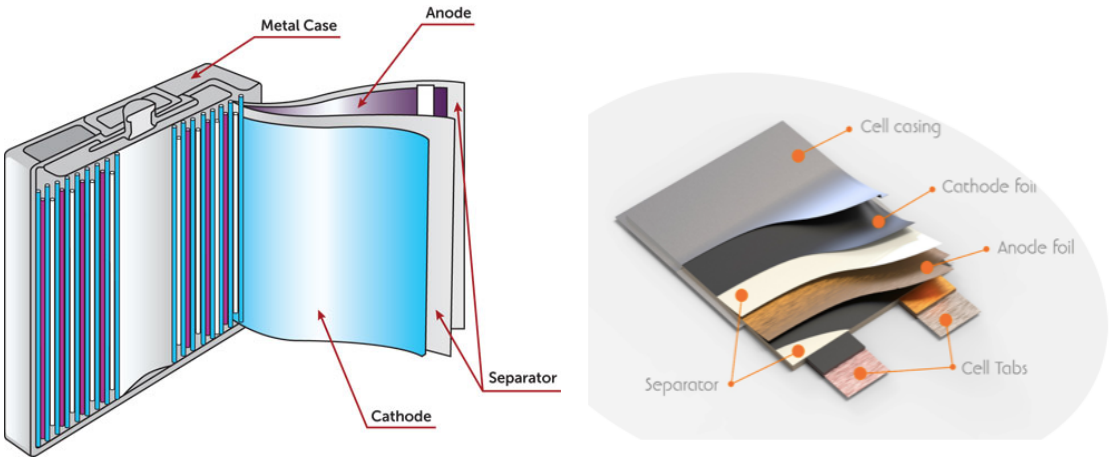

Figure 7. Prismatic (left) and Pouch (right) Cell

highlighted in figure 8.
The most common chemistry adopted in automotive field are the following:

- LCO ($LiCoO_2$): Lithium Cobalt Oxyde is the first generation of cells. It has good specific energy so lower weight for a given energy requirement. Anyway, it is expensive and has some safety issues due to the instability of its components.
- NMC ($LiNiMnCoO_2$): it is the most modern solution and thanks to its combination of Nickel, Manganese and Cobalt, it offers good specific energy and power by keeping a lower cost due to its cheaper materials. It is adopted by some OEM as LG, Samsung, BMW and VolksWagen.
- NCA ($LiNi_{0.8}Co_{0.15}Al_{0.05}O_2$): to improve LCO solution, some Cobalt atomms have been changed with Nickel thus lowering the cost. Aluminum helps in terms of chemical stability so it improves the safety of the cell. This kind of cells is usually employed in OEM as Panasonic or Tesla.
- LMO: an evolution of LCO where Cobalt has been substitued by Manganese. It is cheaper and safer than LCO but overall perfomances are not as high as NMC or NCA types.
- LFP: Lithium Iron Phospate are stable and safe but with a low energy density.

Due to their poor properties compared to the others, the last two types LMO and LFP nowadays are not commonly used in the automotive field.

1.2.2 Working Principle

Lithium-ion batteries employ lithium storage compounds as the positive and negative electrode materials. As a battery is cycled, lithium ion (Li^+) exchange between the positive and negative electrodes, as it has shown in figure 9.

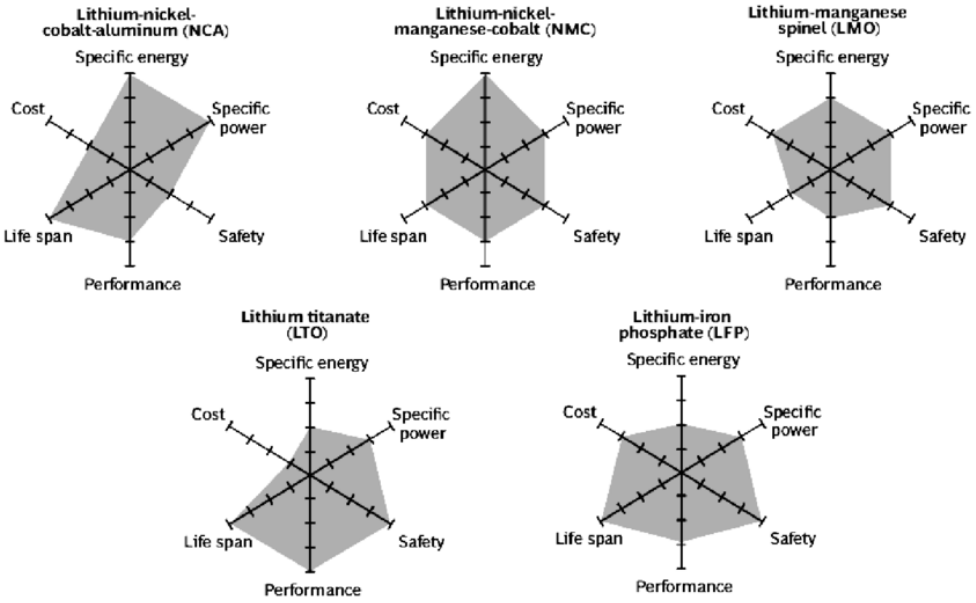

Figure 8. Chemistry Typologies of Li-Ion cells

Li-ion batteries have been referred to as "rocking chair" batteries because the lithium ions "rock" back and forth between the positive and negative electrodes as the cell is charged and discharged.

The cell-operating principles of the different chemistries are similar; $LiCoO_2$ will be described here as an example. The reactions governing this cell chemistry are as follows:

$$Positive\ elctrode\ \ \mathrm{CoO_2 + Li^+ + e^- \underset{\text{Charge}}{\overset{\text{Discharge}}{\rightleftharpoons}} LiCoO_2}$$

$$Negative\ electrode\ \ \mathrm{LiC_6 \underset{\text{Charge}}{\overset{\text{Discharge}}{\rightleftharpoons}} Li^+ + C_6 + e^-}$$

$$Net\ cell\ reaction\ \ \mathrm{LiC_6 + CoO_2 \underset{\text{Charge}}{\overset{\text{Discharge}}{\rightleftharpoons}} LiCoO_2 + C_6}$$

$$E_0 = 3.7\ V\ (Discharge)$$

When the cell is charged, lithium is combined in the anode as LiC_6.

During discharging, the Lithium ions are extracted from the anode throughout a process called " deintercalation mechanism", enter the liquid phase, migrate through the separator and are inserted into the cathode with the metal oxide ("intercalation mechanism").

A key feature of Li-ion cells is that upon initial charge, a surface film or surface electrolyte interface (SEI) layer is formed between the electrodes and the electrolyte. It effectively protects against a perpetual reaction of intercalated lithium with the electrolyte. The growth of this layer is one mechanism for capacity loss and impedance growth of the cell as it ages. Mechanical stress as a result of negative electrode expansion/contraction during battery cycling is another aging and failure mechanism [2].

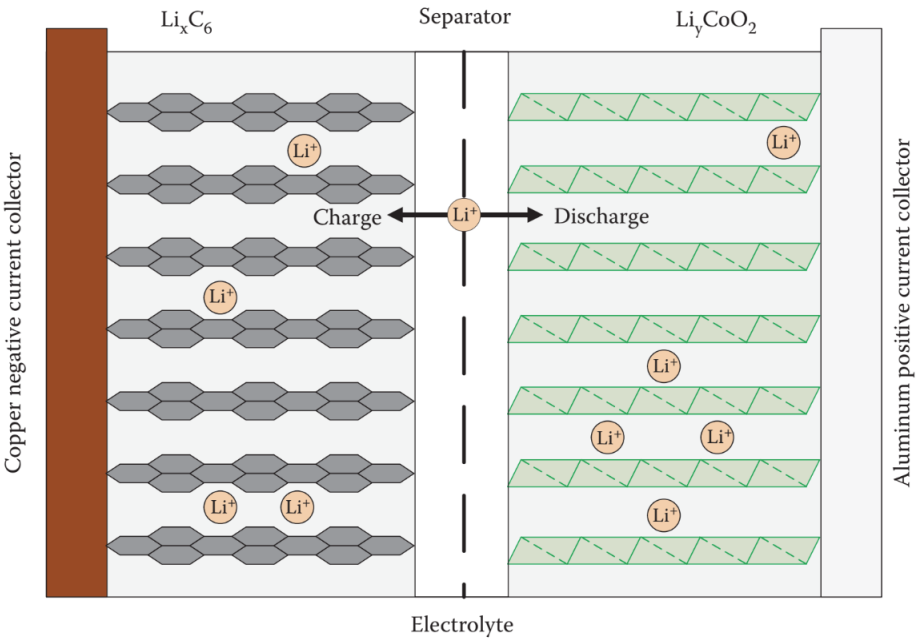

Figure 9. Lithium-ion LCO Cell Working Principle from [2]

1.2.3 Battery Cell Failure Mechanisms

Failure mechanisms are essentially three: overcharge, overdischarge and short circuit. Each one of them has serious effects on the safety of the overall battery.
Overcharge occurs when the battery is charged above defined charge end voltage. It leads to irreversible damage and loss of capacity. Formation of metallic lithium around the anode, called "Lithium plating", is also another consequence of overcharge. Furthermore, above 4.4V, cathode active material starts to break down, leading to exothermic process with generation of heat and oxygen, impacting on the safety of the battery that risk to inflate and, in some cases, blow up (thermal runaway).
Overdischarge below defined discharge end voltage leads to irreversible damage as dissolution of electrolyte and loss of capacity.
When a direct connection between positive and negative terminal of a cell or a battery is created due to, for instance, an overcharge phenomenon, short circuit occurs. This provides a virtual zero resistance path for current flow that can assume really high dangerous values. The most critical effect is the heating of the cell that allows decomposition and evaporation of the electrolyte fluid and the decomposition of the cathode active material. For these reasons, additional heat production and gas formation arise thus potentially leading to the fire of the battery.
Figure 10 shows all the possible issues a battery can encounter during its life, if determined temperature values and delta temperature are reached.
Testing batteries is not always possible both because of time tests require and because, most of the time, these are destructive tests. Because of that, models predicting battery

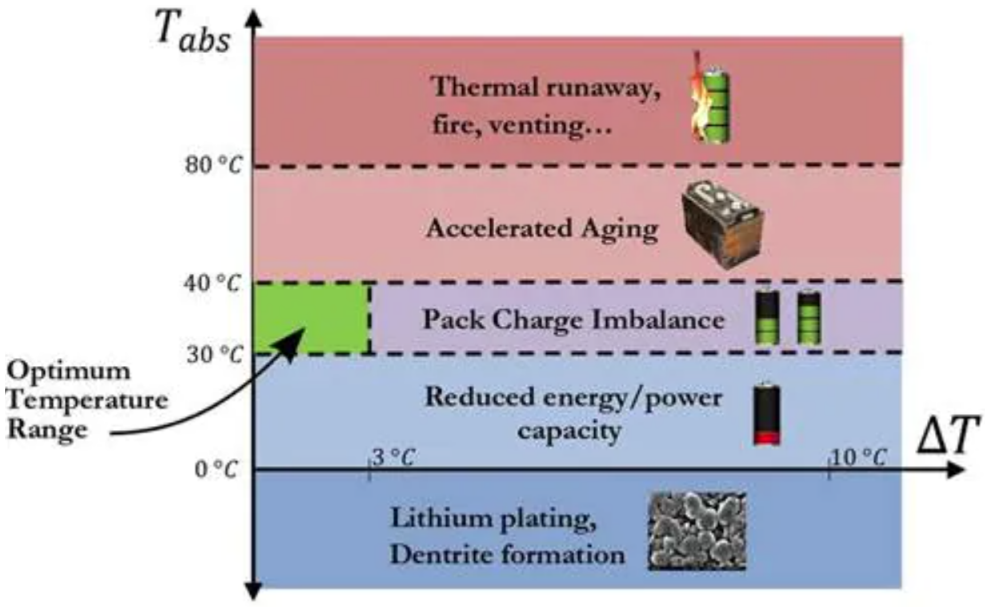

Figure 10. Issues Related to Temperature

temperature by simulating their behaviour under specific current profiles, are essential today to save both in terms of time and cost during the design phase of an EV.
Furthermore predictions from the model can help battery management systems in their functioning, for instance by comparing measured and simulated temperatures, to trigger all the safety procedures.

1.3 Electrical and Thermal Models

Estimation of the battery temperature is a crucial point in the managing of the battery system of a hybrid or pure electric vehicle since it affects its performance and especially its range of autonomy, which is the most important concern for the customers.
To estimate the temperature of a battery, thermal models must take in consideration the generated heat inside the battery due to its electrochemical reactions, as well as the heat transfer exchanged with the environment or with other cells.
Temperature variations leads to change in the battery chemical reactions. These reactions are represented by the parameters in the electrical model such as open circuit voltage, resistors and capacitors whose values are depending on both temperature and state of charge of the battery.

1.3.1 Electrical Models

To assess the performance of a battery, models simulating its output voltage when it is connected to a load are required.

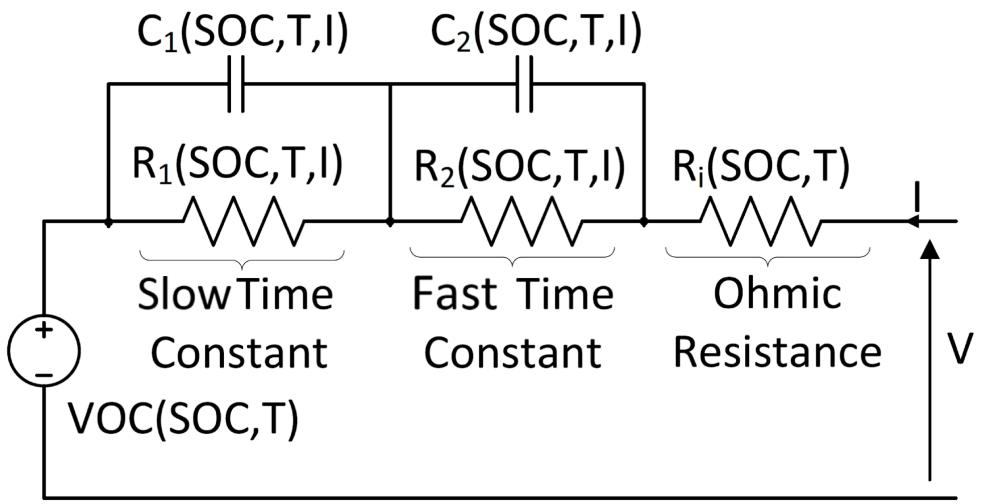

Figure 11. Second Order Equivalent Circuit Model of a battery cell from [4]

Battery models can be roughly divided into electrochemical models, mathematical models and equivalent circuit models.
Although the accuracy of the electrochemical model is high, the structure is complex and difficult to implement, and it is not suitable for modelling actual working conditions.
The mathematical model has a simple structure and is easy to calculate, but it is difficult to describe the external characteristics of the battery [3].
Considering the complexity and accuracy of the battery model, it has been chosen to use a second-order RC equivalent circuit model, also because of its predisposition to be implemented in the MATLAB Simulink environment.
A general schematic diagram of an ECM is shown in Fig.11.

Equivalent Circuit Models

Second order ECM is composed by the following components in series:

- Thevenin's Open Circuit Voltage (V_{OCV}) is represented by an ideal voltage source.
- Internal resistance (R_i) represents the voltage drop of the battery when it delivers/absorbs current at the load.
- Two RC groups (R_1, C_1, R_2, C_2) represent the electrical dynamic behaviours of the battery, through a 1st order's exponential transient.

The OCV value depends on the SOC and temperature of the cell, and the analytic function that relates OCV and SOC can be obtained so that it approximates the cell discharge curve in analysis. Cell discharge curve is usually provided by the manufacturer; as shown for instance in Fig.12.

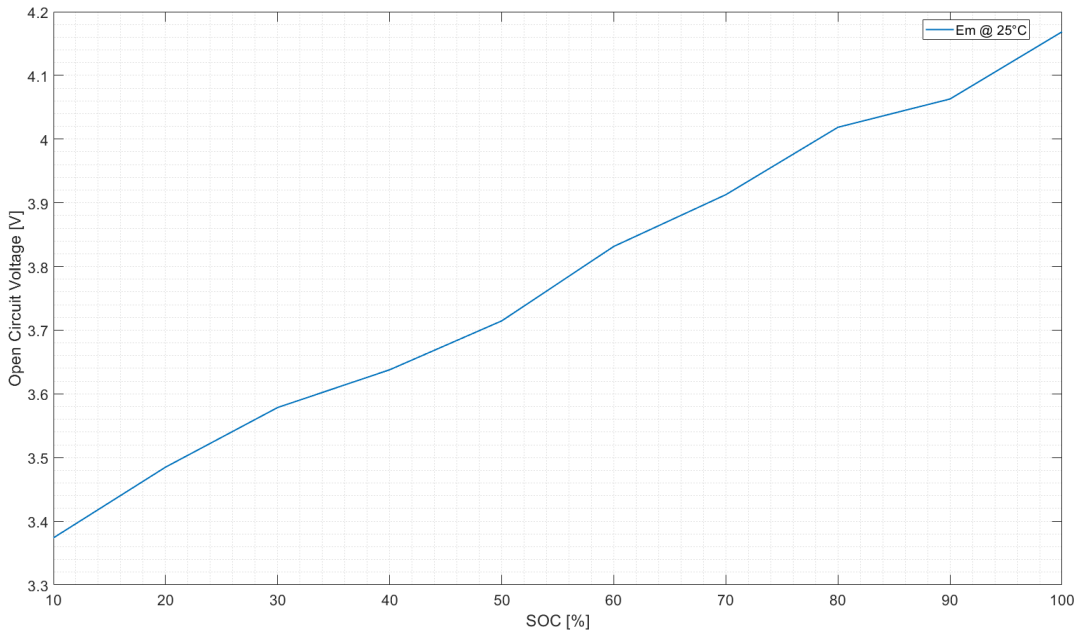

Figure 12. OCV vs SOC at 25°C

Internal resistance R_i value represents the voltage drop of the cell when it supplies/absorbs current at the load. This parameter defines battery performance and its state of health (SOH).

R_1 and C_1 represent the slower dynamics of the cells in order of hours, i.e. the long-term voltage relaxation dynamics [5]. They are more representative of the diffusion processes in the electrolyte and active material.

R_2 is the charge transfer resistance and C_2 represents the electrochemical double layer capacitance describing the electron diffusion dynamics (faster) on the cell's electrodes.

All these parameters are functions SOC of the battery, temperature (T) and current (I) [4].

The transient equation for the voltage computation of one RC branch is:

$$\frac{dV(t)}{dt} = \frac{i(t)}{C_j} - \frac{V_j(t)}{R_j C_j}$$

It has been solved by using the integrator block in Simulink, as showed in figure 13.

Being the equivalent circuit a series of an ideal voltage source, a resistor ad two RC branches in series, the output voltage has been computed by the Ohm's Law as the sum of the contributions coming from each single element, as shown in figure 14 representing the model implemented in Simulink:

$$V_{out} = RI + V_{in} + V_{RC1} + V_{RC2}$$

In the present approach, the battery state of charge has been estimated by ampere-hour integration or Coulomb counting method [6]:

$$SOC = SOC_{t=0} - \frac{1}{C}\int I(t)dt$$

where $SOC_{t=0} = 1$ (when the battery is 100% charged), and C is the nominal capacity of the cell.
To conclude this section, current, SOC and temperature of the battery T_b are the inputs and voltage of the battery is the output V_{out}.

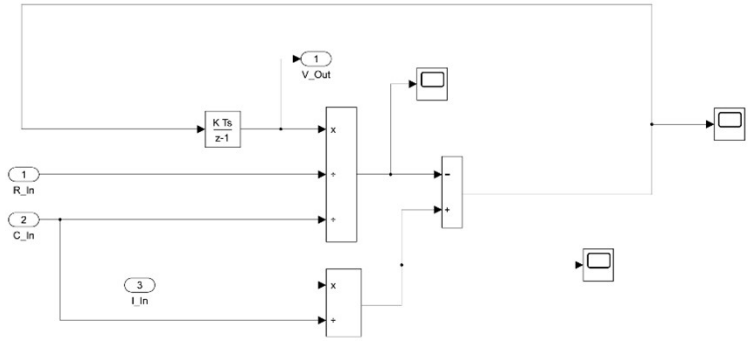

Figure 13. RC Branch Simulink Model

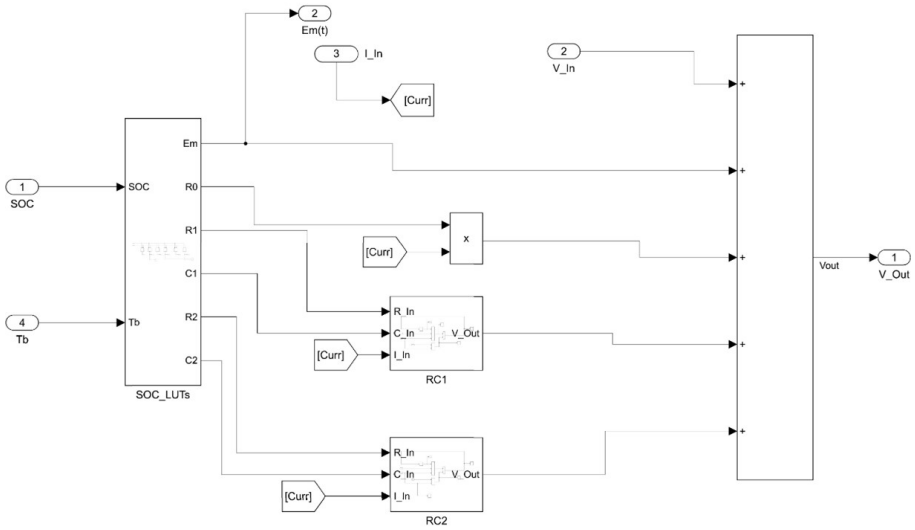

Figure 14. Cell Module Simulink

1.3.2 Thermal Models

The importance of the single temperature lumped parameter model relies in the fact that it can be utilized for real time estimations because of its simplicity and low computational

effort with respect heavy CFD models.
In this way, it can be implemented in ECU of the vehicle for instance to adjust battery cooling strategies and to maximize its performance.
Furthermore, if the model is well calibrated and its results are meaningful, there is no need to carry on testing procedures of batteries which are expensive and time demanding.

CFD Models

The energy equation employed by ANSYS CFD solver to model the battery as a solid is governed by:

$$\frac{\partial(\rho h_e)}{\partial t} + \nabla(V\rho h_e) = \nabla(k\nabla T) + S_h$$

where ρ is the density, $h_e = \int c_p dT$ is the sensible enthalpy, c_p is the specific heat, k is the thermal conductivity, T is the temperature, S_h is the volumetric source term, and the velocity V is obtained from the motion of the fluid.
Being a finite element analysis, this approach requires a well defined CAD geometry of the cell, and final results are strongly affected by the dimension of the mesh which has been employed to discretized the geometry.
The smaller is the mesh, the better are the results but at expenses of computational time which increases. So it is not feasible to implement a model such this for real time estimation of the battery temperature in a car, but it is useful during its design phase.

Lumped Parameters Models

The First Law of Thermodynamics representing the transient energy equation for the single cell is presented in its general form (Fig.15):

$$\rho_b c_{p,b} V \frac{\partial T_b}{\partial t} = q_t - q_{conv} - q_{rad}$$

In this equation, ρ_b is the density of the battery, $c_{p,b}$ is the heat capacity of the battery, V is the volume of the battery, t is the time, while q_t, q_{conv} and q_{rad} are respectively the heat generation inside the cell and the convective and radiative heat transfer terms.
The last two terms have a negative sign because they are exchanging heat with environment thus subtracting heat from the battery, cooling it.

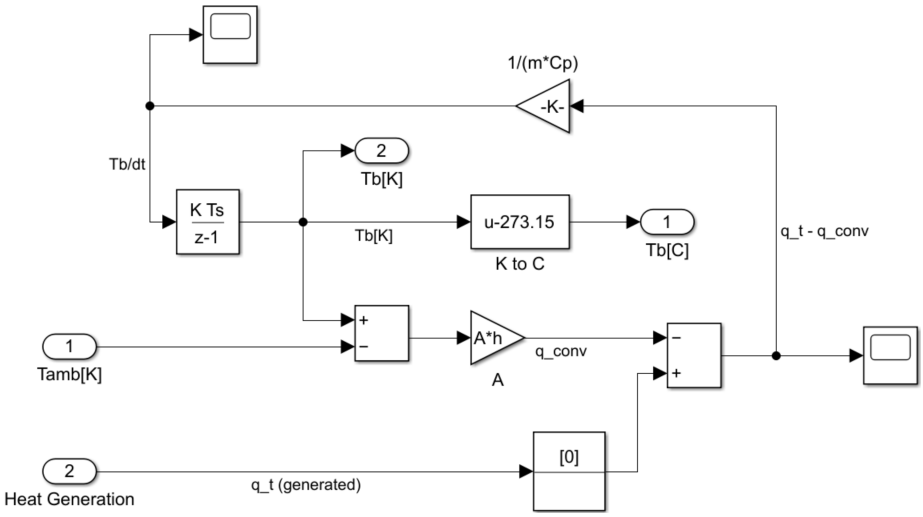

Figure 15. Simulink Energy Balance Equation

The convective heat exchange can be written as

$$q_{conv} = Ah(T_b - T_\infty)$$

where h is the natural convection air heat transfer coefficient, A is the surface area of the cell, T_b is the battery temperature and T_∞ is the steady state ambient temperature.
For what concerns the radiative heat transfer, it can be expressed as

$$q_{rad} = A\epsilon\sigma(T_b^4 - T_\infty^4)$$

being ϵ is the emissivity of the surface of the battery and σ is the Stefan Boltzmann constant.
To solve the energy balance equation, the heat generation term (Fig.16) which is denoted by q_t, inside the battery should be evaluated by adopting the Bernardi's equation [7]:

$$q_t = q_{irrev} - q_{rev}$$

The first term (q_{irrev}) in the heat generation equation stands for the irreversible heat in the electrochemical reaction process inside the Lithium ion battery and is caused by the Joule's heating based on the total internal resistance R.

$$q_{irrev} = I[(V_{ocv} - V_{out}) = I^2R$$

The second term (q_{rev}) is the reversible component of the total heat generation, representing the entropy change attributed to electrochemical reactions [8].

$$q_{rev} = -I[T_b \frac{dV_{OCV}}{dT}]$$

V_{ocv} is the open circuit voltage and V_{out} is the closed circuit voltage of the battery.
"I" denotes the applied current, which is negative during the charging, and positive during the discharging.
By knowing V_{ocv} value in different temperature values and SOC conditions, it is possible to estimate the entropic term parameter.
For simplicity the radiation term of the heat transfer equation has not been implented in the model because no sufficient data were available about the emission coefficient ϵ.
The most important coefficients are $c_{p,b}$ and h but both of them has to be retrieved experimentally.

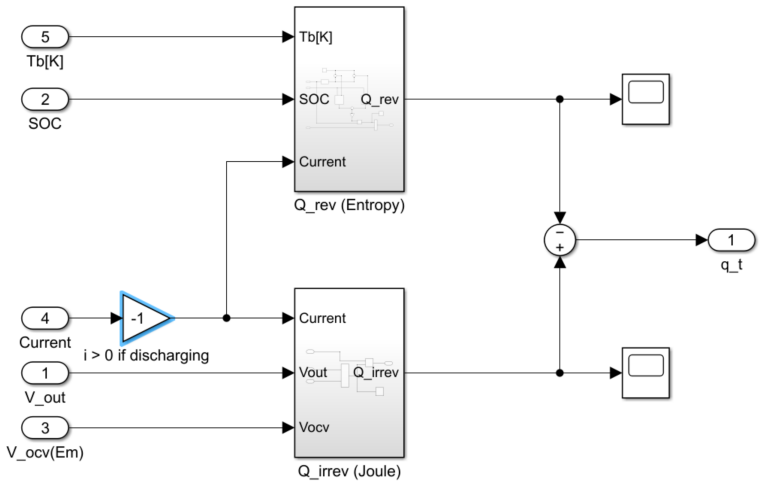

Figure 16. Simulink Heat Generation Model

In this first analysis, to avoid further experiments, their values have been chosen from the literature [9] [10]:

$$4 < h < 12 \, [\frac{W}{m^2 K}]$$

$$700 < c_{p,b} < 2000 \, [\frac{J}{kgK}]$$

By utilizing Parameter Estimator Tool in the Simulink toolbox, it has been discovered that the higher are both coefficients, the better is the estimation of the cell temperature, i.e. the lower is the difference between simulated and experimental temperature signal.
Anyway, this procedure has led to unrealistic values so $h = 7.5 \, [\frac{W}{M^2 K}]$ and $c_{p,b} = 1800 \, [\frac{J}{kgK}]$ have been selected.
For what concern the heat transfer coefficient, the upper constraint has been imposed in a way that natural convection has been respected, without going in the forced convection cooling.

Theoretically, assuming that Biot number of the Lithium Ion battery tested is below 0.1, thus under natural convection conditions, the most accurate method to compute the average heat transfer coefficient around the battery is given by the empirical correlation by Churchill and Chu based on the long horizontal approach [11]:

$$h = \frac{Nu_D * k_b}{D}$$

$$Nu_D = \{0.6 + \frac{0.387 Ra_D^{\frac{1}{6}}}{[1 + (\frac{0.559}{Pr})^{\frac{9}{16}}]^{\frac{8}{27}}}\}^2 \, , Ra_D \leq 10^{12}$$

$$Ra_D = \frac{g\beta(T_b - T_\infty)D^3}{\theta\alpha}$$

where h is the convective heat transfer coefficient, k_b is the conductive heat transfer coefficient, Nu_D is the Nusselt number, D is the diameter of the cylinder, Ra_D is the Rayleigh number, Pr is the Prandtl number, g is acceleration due to gravity, β is the thermal expansion coefficient, T_b is the surface temperature, T_∞ is the air temperature, θ is the kinematic viscosity, and α is the thermal diffusivity.
In this case, h, Nu_D and Ra_D numbers are calculated at average temperature $\frac{(T_b - T\infty)}{2}$.
Instead k_b, θ, α and Pr are the properties of material to be extracted from thermodynamic tables and should be introduced as a look up table in Simulink project.
The main issue with these parameters is that they are almost unreachable, unless an extensive study on that specific kind of battery had been carried out.
Regarding the specific heat of the battery, since it is an intrinsic property of the cell, it has been chosen in order to have a reasonable fitting between experimental measurements and modelled temperatures.

2. Single Cell Analysis

The aim of the first part of the thesis is to create a temperature parameter model for the single battery cell Samsung IN21700-30T starting from its equivalent circuit model (ECM) with two RC branches, using MATLAB and Simulink environment.
Once the ECM has been implemented, the generated heat inside the cell while it is working under some charge/discharge cycle can be retrieved through the known formula of the dissipated power in the battery by joule effect.
Then a convective heat exchange between the cell and the air of the environment has been considered and, by the thermodynamic equation of energy balance, the temperature of the cell has been computed.
Finally, computed temperature has been compared with the measured temperature on the surface of the cell whose experimental data has been provided by the literature.

In the first section of this chapter, a description of the analysed battery cell whose experimental data has been adopted is necessary in order to adjust the ECM.

In the second section, the typical testing procedure allowing battery perfomance characterization is analysed.

Parameter identification procedure to optimize the internal parameters of the ECM according to mathematical algorithm is discussed in the third section of this chapter.

2.1 Cell Data

Samsung IN21700-30T (Fig.17, Table 2) is a Lithium Iron Phosphate cell that has been selected for the first trials of simulations since it has been already studied and whose results coming from various test procedures are available in the literature [1].
The results of tests on the battery have been saved in a file.mat whose data colums have been named:

- Time (time in seconds);
- TimeStamp (timestamp in MM/DD/YYYY HH:MM:SS AM format);
- Voltage (measured cell terminal voltage, sense leads welded directly to battery terminal);
- Current (measure current in amps, HPPC profile);

- Ah (measured amp-hours, with Ah counter typically reset after each charge, test, or drive cycle);
- Wh (measured watt-hours, with Wh counter reset after each charge, test, or drive cycle);
- Power (measure power in watts);
- Battery_Temp_degC (battery case temperature, at middle of battery, in degrees Celsius measured with a AD592 +/-1degC accuracy temperature sensor).

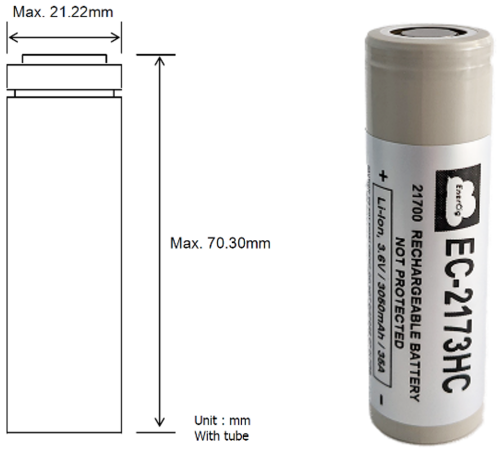

Figure 17. Battery cell Samsung IN21700_30T

Geometry	Cylindrical	-
Height (max)	70.3	mm
Diameter (max)	21.22	mm
Weight (max)	69	g
Maximum Voltage	4.2	V
Nominal Voltage	3.6	V
Nominal Capacity	3	Ah
Maximum Continuous Discharge Current	35	A
Maximum Non Continuous Discharge Current	14.7	A
Recharge Maximum Current	10	A
Discharge Cut-off Voltage	2.5	V
Discharge Temperature Operative Range	[-20 60]	°C

Table 2. Samsung IN21700-30T cell characteristics

These tests have been saved with a 0.1 second time step, meaning with a sampling frequency of 10 Hz.

Figure 18 and figure 19 shows the acquired data just mentioned.

In particular it can be noticed at the end of the test, a final charging phase which has not been considered because of some issues related to the ECM.

The final plot of the temperature shows the experimental data that will be utilized to

validate the thermal model of the single cell.
The various oscillations in the experimental measured temperatures probably are due to acquisition noise from the measurements.

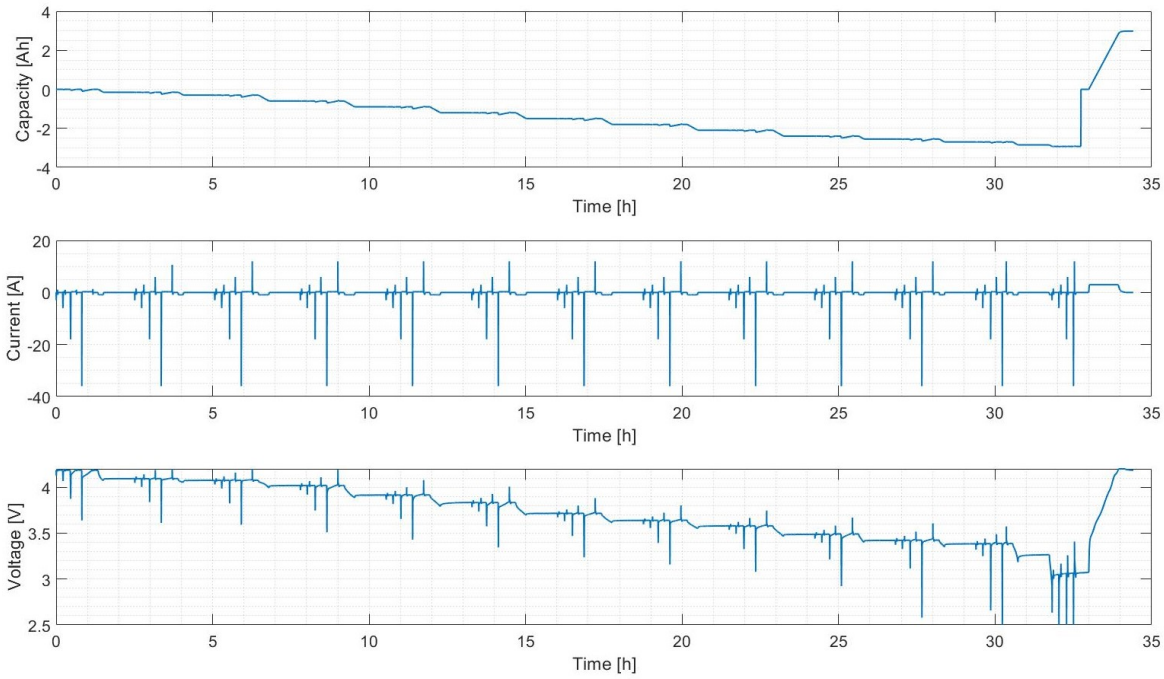

Figure 18. Dataset at 25°C: Capacity - Current - Voltage.

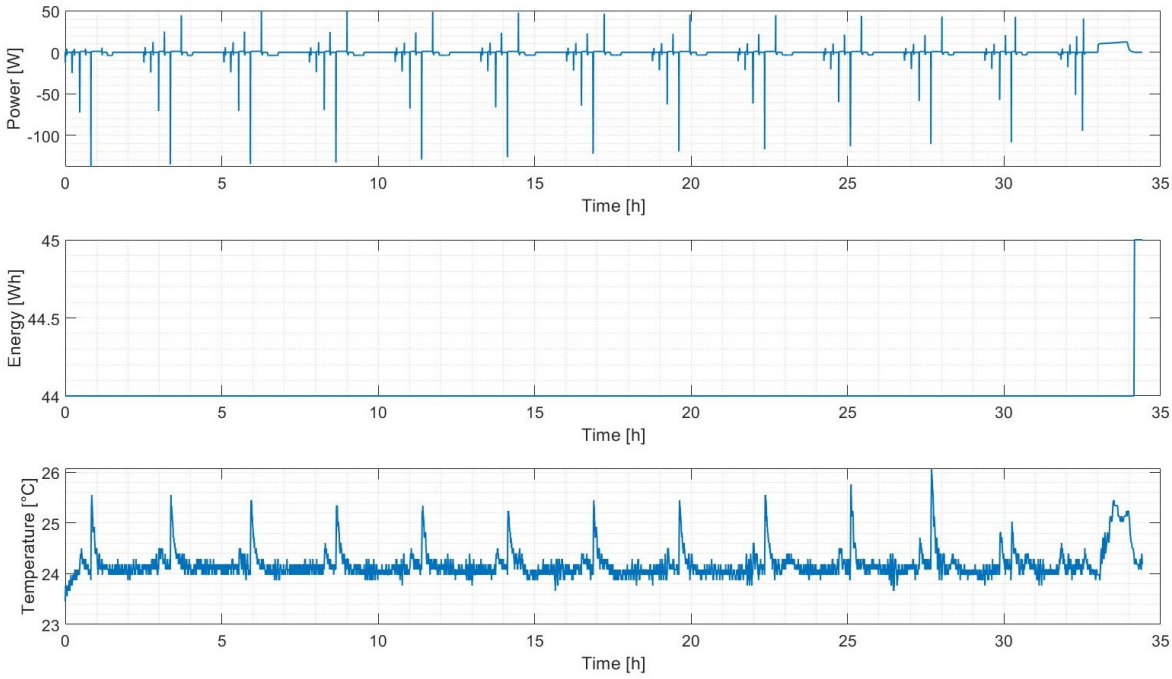

Figure 19. Dataset at 25°C: Power - Energy - Temperature.

2.2 HPPC Test

From the experimental data provided by the literature, just Hybrid Pulse Power Characterization (HPPC) tests have been considered.
This is a commonly employed method to evaluate the dynamic properties of a battery.
The battery is charged and discharged under a controlled condition and the terminal voltage, current and temperature measurements are monitored.
Different working conditions of a battery can be simulated by considering different C rates at which a battery is charged or discharged.
C rate is the ratio between the load at which the battery is connected, usually referred as a current (I_{bat}) in Ampere, and its nominal capacity (C_{bat}) that is usually expressed in Ampère-hour: discharging a battery at 1 C rate means that the battery is completely discharged in 1 hour.

$$c = \frac{|I_{bat}|}{C_{bat}} \, [\frac{1}{h}]$$

A typical HPPC test profile is shown in Fig.20: first a charging phase is carried on, then a long rest period where OCV is measured occurs. After that, a short discharging and a charging phase lasting about 10 seconds are performed at different C rate according to the characteristic of the battery and according to the established experiment.

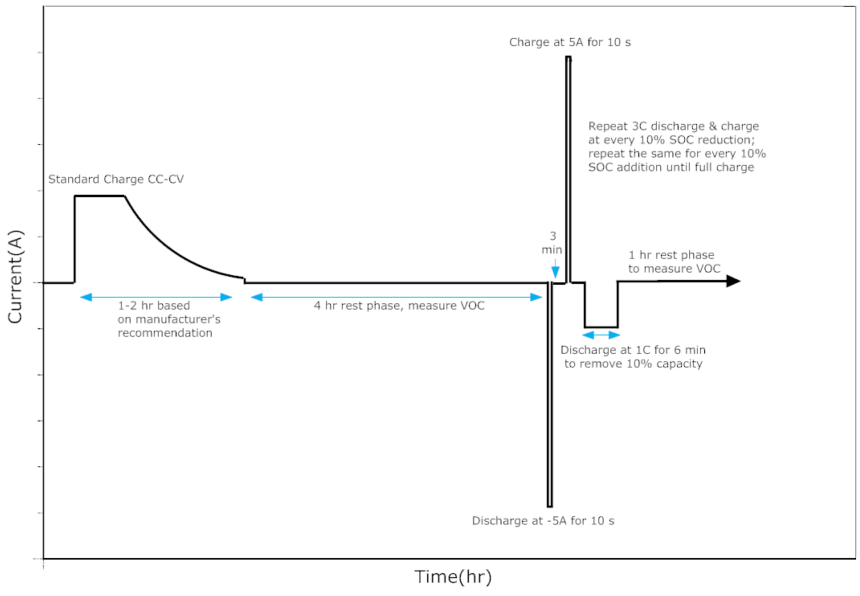

Figure 20. Reference HPPC from [4]

Instead figure 21 shows measured current and tension of the studied cell at ambient temperature of 25°C.
It consist in four pulse discharge HPPC tests at 1, 2, 6, and 12C discharge and 0.5, 1, 2,

and 4C charge, performed at 100, 95, 90, 80, 70..., 20, 15, 10, 5, 2.5 % SOC at temperature of -20°,-10°,0°, 10°, 25° and 40°C [1].
The discharge pulse is further split into the short time constant τ_2, representing the fast dynamics, and the long time constant τ_1, representing the slow dynamics.

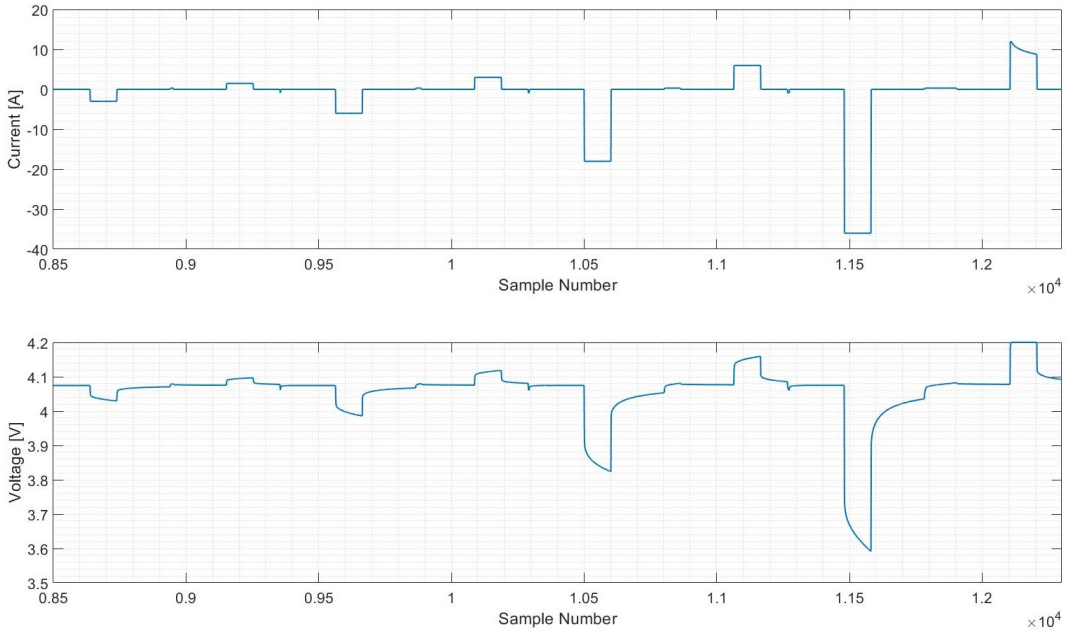

Figure 21. HPPC profile at 25°C

2.3 Parameter Identification

Inside the ECM there are several parameters as V_{OCV}, R_0, R_1, R_2, τ_1 and τ_2 that characterize the performances of a battery. Their behaviour is not constant but it varies dramatically based on the operating conditions in the states of the battery such as SOC and temperature. For this reason, to obtain more accurate results concerning battery output voltage V_{out}, a procedure of parameter optimization has been carried out.
It is an optimization procedure in which the objective function to be minimized is the error function between simulated voltage by the model and the experimental battery voltage from literature data.
This is done by changing the ECM parameters as resistor, capacitor and OCV values until experimental voltage and simulated voltage by the ECM model match.
By using MATLAB Signal Processing Toolbox in combination with the Parameter Estimator tool, part of Simulink Design Optimization, the parameters of the ECM have been automatically tuned to match the battery measured data.
Starting from predefined values, at each SOC level and for a defined environmental temperature, the code compares the two voltage signals by running the ECM each time

with values of the parameters slightly different, until the error between experimental and simulated signal is sufficiently small.
Thus the results of the code are the optimized ECM parameters for each SOC at the given temperature.
By repeating this process for other temperatures, a set of parameters is obtained as function of both SOC and different ambient temperatures.
In this way, 2D look up tables can be implemented in the ECM model (Fig.22) thus providing the dependency on the temperature of each parameters and so improving the initial model where parameters were depending just on the SOC.
Finally these tables have been arranged into matrices 10 by 6 because it has been chosen to simulate 10 SOC levels [0.1, 0.2, 0.3, 0.4, 0.5, 0.6, 0.7, 0.8, 0.9, 1] (rows) at 6 environmental temperatures [-20°, -10°, 0°, 10°, 20°, 40°C] (columns).

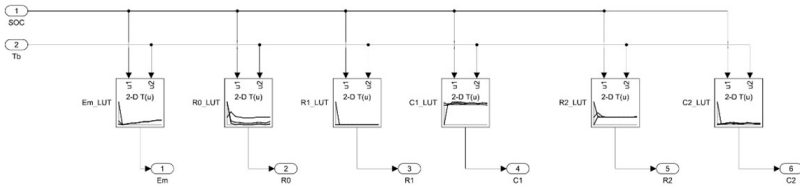

Figure 22. 2D Look Up Tables Simulink

It has been chosen to discard the first SOC value corresponding to 0.01% because both the optimization procedure has not properly worked at that SOC level and because, normally, such SOC level are not reached by a battery in normal working conditions.
Furthermore, to make the procedure functioning, input data have been filtered and cleaned because of their not always perfect sampling: in some points data were sampled without a constant sample rate resulting in some repeated equal values.
Then after having deleted unnecessary data, they have been interpolated again with a constant sampling rate to reconstruct a cleaner input signal.

2.3.1 Mathematical Outlines

An optimization procedure is a process where an objective function, must be minimized or maximized. This objective function is depending on some control variables which constitute the algebraic space R_n, of n dimensions represented by n variables.
During the inizialitazion, a point in the space of variables is selected; it works as a starting point from which the algorithm starts to evaluate the optimal values of the variables that satisfy the imposed target.
So the two most important things to be defined are the objective cost function and the

adopted algorithm to move in the space of variables.
Since our problem involves the minimization of the error among the measured and the modelled voltage signals, the objective function chosen for the optimization has been the "NLSqnonlin" (Non-linear Least Square).
It solves nonlinear least squares curve fitting problems of the form [12]:

$$\min_x ||f(x)||_2^2 = \min_x(f_1(x^2) + f_2(x^2) + ... + f_n(x^2))$$

The method exploited in Optimization Toolbox™ solvers is based on trust regions, a simple yet powerful concept in optimization.
To understand the trust-region approach to optimization, unconstrained minimization problem must be considered, where f(x) must be minimized: this function takes vector arguments and returns scalars.
The starting current point is x in n-space and it has to be improved by moving to a point with a lower function value.
To do so, the algorithm approximates f with a simpler function q, which reasonably reflects the behavior of function f in a neighborhood N around the point x. This neighborhood is the trust region.
The solver computes a trial step s by minimizing (or approximately minimizing) over N. The trust-region subproblem is

$$\min_s q(s), s \in N$$

In this way, the solver updates the current point to $x + s$ if $f(x + s) < f(x)$; otherwise, the current point remains unchanged and the solver shrinks N (the trust region) and repeats the trial step computation.
In the standard trust-region method, the quadratic approximation q is defined by the first two terms of the Taylor approximation to F at x. The neighborhood N is usually spherical or ellipsoidal in shape. Mathematically, the trust-region subproblem is typically stated

$$min(\frac{1}{2}s^T Hs + s^T g \ : ||Ds|| \leq \Delta)$$

where g is the gradient of f at the current point x, H is the Hessian matrix (the symmetric matrix of second derivatives), D is a diagonal scaling matrix, Δ is a positive scalar, and $||...||$ is the 2-norm [13].
The solution of this equation involves some mathematical problems that are outside the topic of this thesis and whose dissertation will not be explained.

2.4 ECM Inizialization

Regarding the initial ambient temperature setting T_∞, it has been chosen to select and average the first 2000 measured values from experimental data, in order to obtain an initial value corresponding to the real temperature of the cell during the first instants of the experiment.
Since data relative to the rated capacity of the cell have been provided by experimental measurements [1], another method has been implemented in the Simulink model to evaluate SOC.
State of charge has been computed as the difference between discharge capacity and rated experimental capacity, than normalized by the nominal capacity C of the cell as function of temperature (Table 3, represented by 1D look up table in the Simulink model) and at the end constrained with a saturation block to avoid SOC unrealistic values (Fig.23).

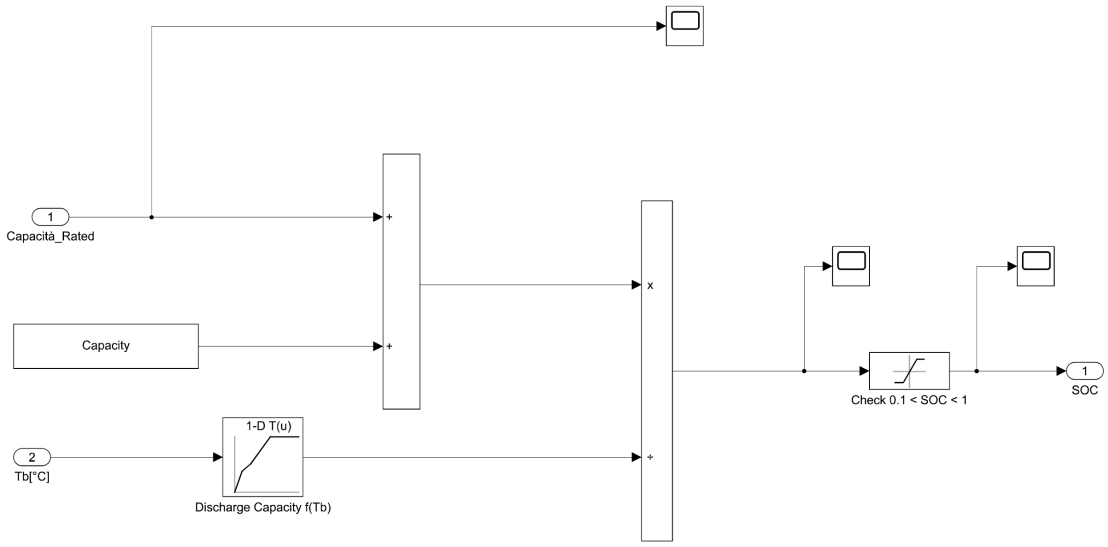

Figure 23. SOC estimation model

-20°C	-10°C	0°C	25°C	60°C
60 %	75 %	80 %	100 %	100 %

Table 3. Temperature dependence of discharge capacity

For what concern the entropic term $\frac{dV_{ocv}}{dT}$, firstly, it has been computed by making the concatenated derivative since both the derivative of voltage $\frac{dV_{ocv}}{dt}$ and derivative of temperature $\frac{dT}{dt}$ in time were already provided by the model:

$$\frac{dV_{ocv}}{dT} = \frac{dV_{ocv}}{dt} * \frac{1}{\frac{dT}{dt}}$$

Anyway, the derivative block in Simulink has shown a weird behaviour with strange oscillations probably due to some mathematical questions. These oscillations have caused some problems in the model that, as results, has provided meaningless values of temperatures. To solve this issue, it has been chosen to compute the derivative with an incremental ratio by exploiting the output of the 2D look up tables, in particular the one regarding open circuit voltage as function of SOC and temperature (Fig.24).

$$\frac{dV_{ocv}}{dT} = \frac{V_{ocv}(T+0.5)|_{SOC} - V_{ocv}(T-0.5)|_{SOC}}{0.5+0.5}$$

It has been also carried out an in-depth analysis to assess the sensitivity of the incremental ratio with respect the increment, that showed a stronger relevance in case of an increment equal to 4°C.

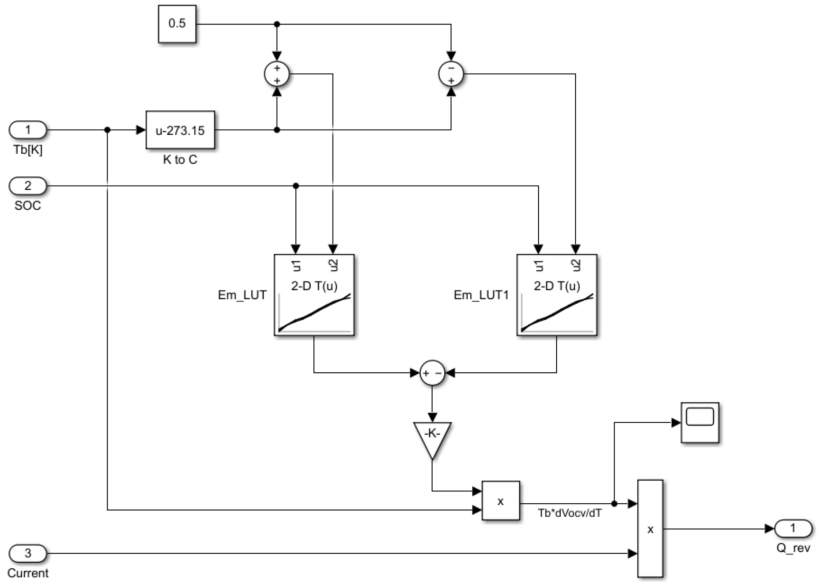

Figure 24. Reversible Entropic Heat Term Computed With Incremental Ratio

3. Battery Rack Analysis

The third chapter of this thesis is going to analyse all the steps necessary for the development of a battery model made by 25 cells, organized into 5 rows of 5 cells each.
Being all the HPPC cycles more or less the same, it has been arbitrarily chosen to simulate the model with the data-set provided by the literature [1] at the temperature of 25°C.
For these kind of models, instead of Simulink environment, Simscape one has been considered the most appropriate, since its easier implementation at the expenses of computational time that slightly increases with respect a purely numerical Simulink model.
Simscape™ enables a rapidly creation of physical systems models by assembling fundamental components into a schematic.
The built models are based on physical connections and the system level equations are automatically determined by Simscape.

In the first section of this chapter, a comparison between the single cell model developed with Simscape and the one developed with Simulink has been carried out in order to assess if the two methodologies of work were similar and if they provided the same results.

The second section is focused on the development of one row made out of 5 cells, to discover how they interact each other and to state which is the most correct way to implement heat exchange among them.

Finally a simplified battery model made out of 5 rows has been developed in the last section of this chapter.

3.1 Simscape Single Cell Model

To effectively assess if using Simscape provides the same results as using Simulink, a Simscape model of the single cell has to be built.
Differently from Simulink, that is based on the resolution of numerical equations, in the Simscape environment the two parts of the model can be separated because of the different nature of physical connections, i.e. the electrical ones and the thermal ones.
These physical signals must be measured with sensor blocks and then they must be converted into Simulink signals by the PS-Simulink converter block (white and black triangles) to be able to visualize and exploit them using Matlab.
In figure 25, it can be noticed both the electrical path in blue and the thermal part in orange;

also voltage sensor to extract the voltage signal from the circuit can be seen, as well as the current source block that exploits the data-set coming from the Matlab environment, thus generating the current input for the battery model.
Converting the physical signals is useful also to implement Simulink blocks when they are required.
For instance when an initial condition has to be set in order to avoid algebraic loop, which is a common issues encountered while constructing these kind of models, an initial condition block directly taken from the Simulink library can be implemented, thus resolving the loop.
Or, as another example, being the thermal connections set to give as outcomes temperatures in Kelvin Degree, a simple bias block to convert temperatures into Celsius Degree can be implemented.

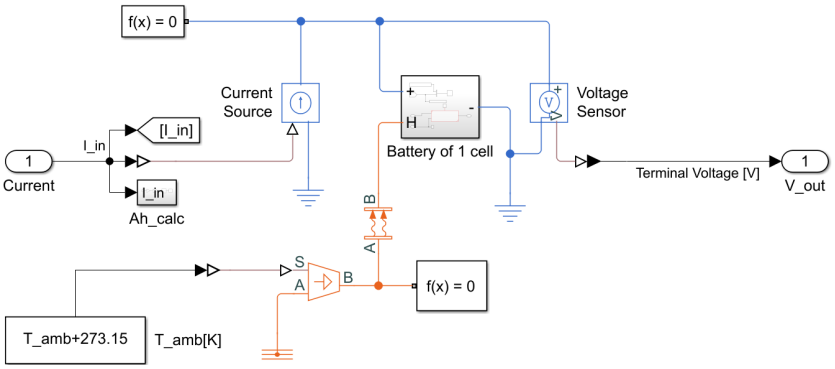

Figure 25. Simscape Battery Layout

3.1.1 Electrical Circuit

Regarding the electrical part, it does not differ from the equivalent circuit model already explained in chapter 1 as general layout: there are a voltage source representing the open circuit voltage, one resistor representing the voltage drop of the battery when connected to a load and two RC branches, simulating the electrochemical transient behaviour of the battery.
The only difference is that in the Simscape model, various component blocks has been defined such that for a certain input, the block provides an electrical output following characteristic equations of resistor or capacitor.
Furthermore, to compute the dissipated power by Joule effect, that has been used as input for the thermal model since it represents the generated heat inside the battery, also an additional output to the resistor blocks has been defined, according Ohm's Law:

$$Capacitor\ current\ i = C\frac{dV}{dt}$$

$$Resistor\ voltage\ v = R * i$$

$$Resistor\ power\ pow = v * i$$

The inputs for all the components blocks of the electric circuit have been provided by the 2D look up tables, whose values are the same exploited for the single cell ECM, obtained from the parameter identification procedure.
For what concerns the state of charge, since capacity data for the single cell were already provided by the literature [1], instead of the simpler Coulomb counting method, it has been adopted the same method already explained in chapter 2, section 2.
Figure 26 shows the single cell model built using Simscape.

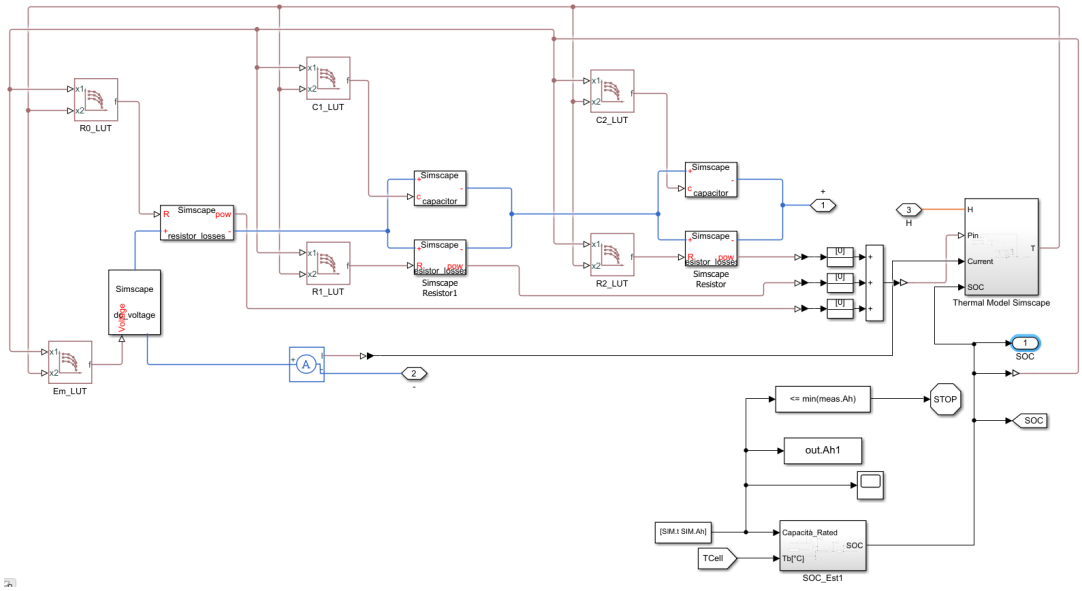

Figure 26. Simscape Single Cell Model

3.1.2 Thermal Model

The thermal model of the single cell consists in four components taken directly from the Simscape library:

- thermal mass;
- controlled heat flow source;
- temperature sensor;
- thermal reference.

The first element models internal energy storage in a thermal network, thus characterizing the thermal behaviour of the analysed body, in this case the single battery cell.
Parameters to be set are the mass and the specific heat of the body, while the variables are

the temperature and the heat flow rate.
Since the heat flow rate (H) has been imposed outside the cell model, as it will be explained later, the only variable to be decided is the temperature, whose initial values has been set in order to start the simulation from the exact temperature of the cell at rest in the ambient, before it has undergone the HPPC cycle.
The controlled heat flow rate block represents an ideal energy source in a thermal network that can maintain a controlled heat flow rate regardless of the temperature difference. Heat flow rate is set by the physical signal port S. A positive heat flow rate flows from port A to port B.
It has been implemented in order to consider the power losses due to Joule effect (Pin) as an heat source that is heating the battery.
Temperature sensor block is necessary to extract the temperature in Kelvin Degree from the thermal network. The measure is positive when the temperature at port A is greater than temperature at port B.
Since these last two blocks characterize the direction of the heat flow rate or the temperature once a thermal difference has been imposed, they both require a thermal reference block.
Thermal reference block represents a reference point in the thermal network where temperature is equal to absolute zero.
The last Simulink bias block has been used to convert the temperature from Kelvin to Celsius Degree because of the dependency of parameters inside 2D look up tables on temperature in Celsius Degree.
To resume, inputs of the thermal model are the convective heat transfer (H) coming from the environment and the power losses (Pin) coming from the ECM, while the output is the temperature in Celsius Degree as it can be noticed in figure 27.

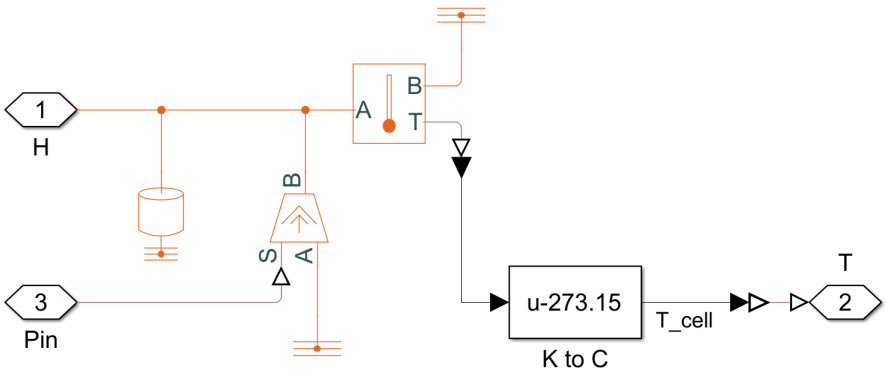

Figure 27. Simscape Themal Model, No Entropy

Convective heat transfer from the environment has been set by implementing an ideal temperature source representing the environmental temperature connected to a convective

heat transfer block outside the cell model as it can be noticed in figure 25.
That block models heat transfer in a thermal network by convection due to fluid in motion according to the equation:

$$Q_{convective} = h * A * T$$

The parameters to be set inside it are the area of the cell and the convective heat transfer coefficient.
In particular the area will be the most important parameter to pay attention at when the interactions between different cells or between cell and environment will be considered in the next sections.
Due to some difficulties in the implementation of the entropic term regarding the heat generation inside the cell, it has been chosen to neglect it throughout the dissertation of the battery model construction using Simscape.

3.2 Row of 5 Cells in Series

Before starting the construction of the overall battery model, it is first necessary to build the model of five cells in series, in order to understand how to organize the various heat transfer among cell to cell and between cell and environment.
Figure 28 shows the Simscape model of a row made out by 5 cells linked in series, whose thermal interactions are only of convective nature.

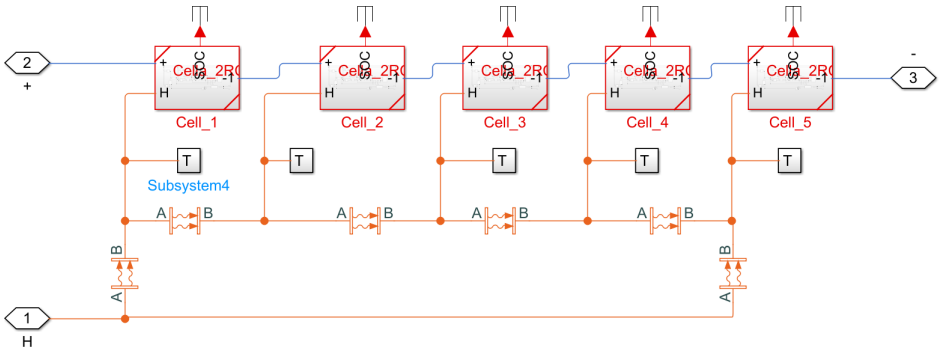

Figure 28. Simscape 5 Cells in Series, Convective Heat Transfer

The two convective heat transfer blocks at the extremities of the row represent the heat transfer between cell and environment, while the blocks in the middle represent the exchanged heat among inside cells.
In this example, it has been supposed the inside cells are not exchanging heat with the environment, as it can be seen there are not heat transfer blocks connected to the environment temperature bottom line.
Differently from the single cell case, where only natural convection between cell and

ambient has been considered, in this case also the conduction among cells can be taken in consideration.
In the Simscape library, it is present the heat conduction block which models heat transfer in a thermal network by conduction through a layer of material.
The rate of heat transfer is governed by the Fourier's Law and is proportional to the temperature difference, material thermal conductivity λ, area normal to the heat direction, and inversely proportional to the layer thickness s:

$$Q_{conductive} = \frac{\lambda A}{s} \Delta T$$

Concerning the electrical equivalent circuit model, it is the same employed in the single cell analysis except for the SOC computation that has been estimated by the Coulomb counting method already explained in chapter 1, to keep the model as general as possible in case experimental data about capacity of the cell would have not been available.
Also HPPC current profiles representing the input data have been kept the same.

3.2.1 Thermal Conductivity

Thermal conductivity is one of the most complex property of a battery to be analysed since its characterization requires lots of experiments and it is an expensive time consuming procedure.
It is widely accepted that two types of thermal conductivities, namely isotropic thermal conductivity and anistropic thermal conductivity have been generally employed in battery thermal models [14].
For Lithium ion batteries, usually it is preferred to embed models with anisotropic thermal conductivity, due to the multilayer structure of that kind of batteries.
This is split into the in-plane or axial thermal conductivity, parallel to the layers, and the cross-plane or radial thermal conductivity, perpendicular to the layers.
Table 4 resumes some of the results related to the thermal conductivities of a Litihium ion battery with a $LiFePO_4$ cathode that can be found in the literature [14].
If anisotropic thermal conductivity had been considered, another typology of thermal model with thermal resistances following the electrical analogy, would have been necessary.
For this reason, since it has been chosen to embed the thermal model with heat transfer blocks instead of thermal resistances, an average value of isotropic thermal conductivity has been considered:

$$\lambda_{isotropic} = 3\ [\frac{W}{mK}]$$

This value is not a fixed one but it could be considered as a parameter to be calibrated if a validation opportunity with experimental data would have been available.

$\lambda_{isotropic}$	λ_{axial}	λ_{radial}
0.666	2.7	0.9
0.98	12	0.34
2.73	21	0.8
3	76	0.4

Table 4. Thermal Conductivities $[\frac{W}{mK}]$ of Lithium-ion Battery, LiFePO4 Cathode

3.3 Simplified Battery Layout

It has been chosen to build a simpler battery model made out by 25 cells arranged in a configuration with 5 independent rows connected in parallel, made of 5 cells in series each as it can be seen in figure 29.

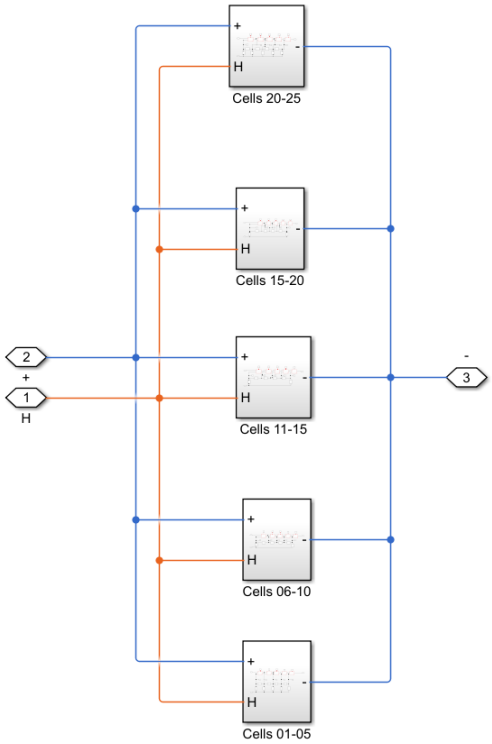

Figure 29. Simscape Battery Pack Layout

Independent because it has been decided to simulate the heat transfer among each cell of the single row but not the ones among cells of different rows, to avoid a too much complex model that would have required a long computational time.
Layout of the battery rack has been designed in a way that its overall envelop would have

been the smallest as possible.
By doing this, rows of cells are slightly misaligned, in order to maximize the contact points among them, as shown in figure 30 where green dots represents contact points between cells and environment, while red dots represents contacts among different cells.

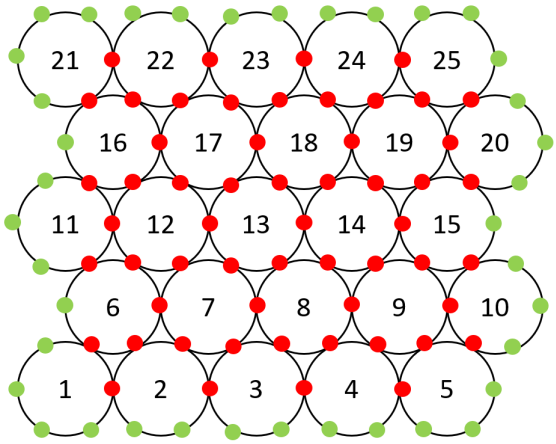

Figure 30. Battery Pack Layout, Top View

The bottom and upper rows have been supposed to exchange heat not only among their cells but also with the environment since they are at the the extremities of the imaginary battery pack.
In figure 31, it can be noticed the model of end rows where for each cell a convective heat transfer block linked to the environment temperature line has been implemented.

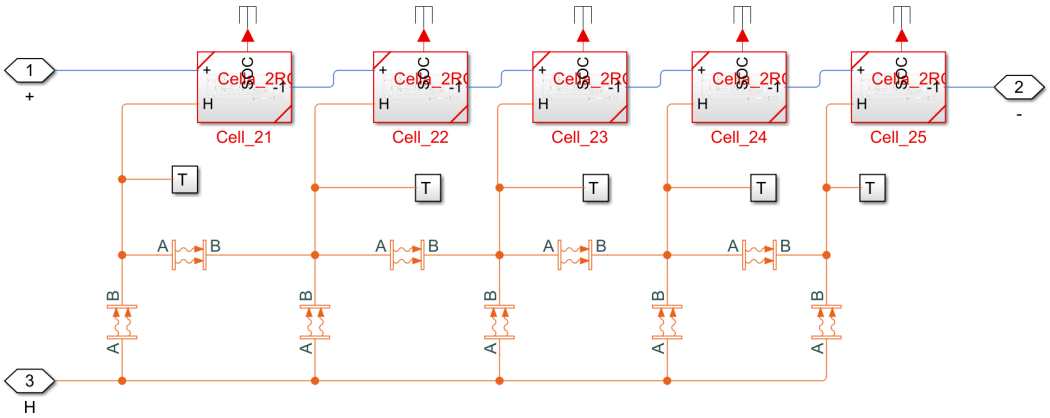

Figure 31. Simscape End Row Layout

Instead, the cells of the three inside rows are exchanging heat among each other, a part from the outside cells of each row that are interacting also with the environment.
Figure 28, shows a configuration of an inside row, where only convective heat transfer

among cells has been considered.
The single cell block is the same analysed in the previous section of this chapter, in particular the one of figure 26.
To simulate conduction among adjacent cells, the conduction block must be placed in between two cells, as it is shown in figure 32.
In all these models, the involved area in the heat exchanges have been supposed to be only the lateral surface of the cell.

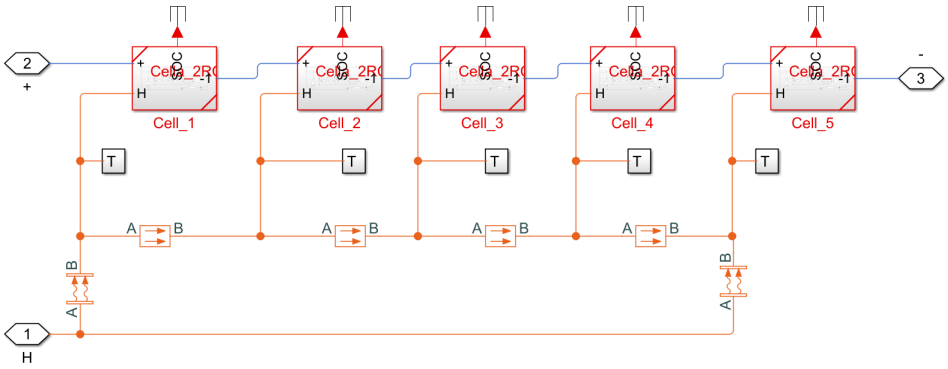

Figure 32. Simscape Row, Conduction

4. Results

4.1 Single Cell Results

In the first part of this section, the results given by the optimization procedure have been reported by plotting them in a surface form representing the 2D look up tables of the parameters implemented in the ECM (Fig.33). Also some statistical parameters as root mean square error and residuals have been reported to assess the coherence of the obtained results.

Then, the outputs of the ECM model such as state of charge and output voltage have been showed in the second part.

Finally, in the last part, temperature profiles of the cell under different HPPC test cycles have been presented and compared with the experimental data coming from the literature.

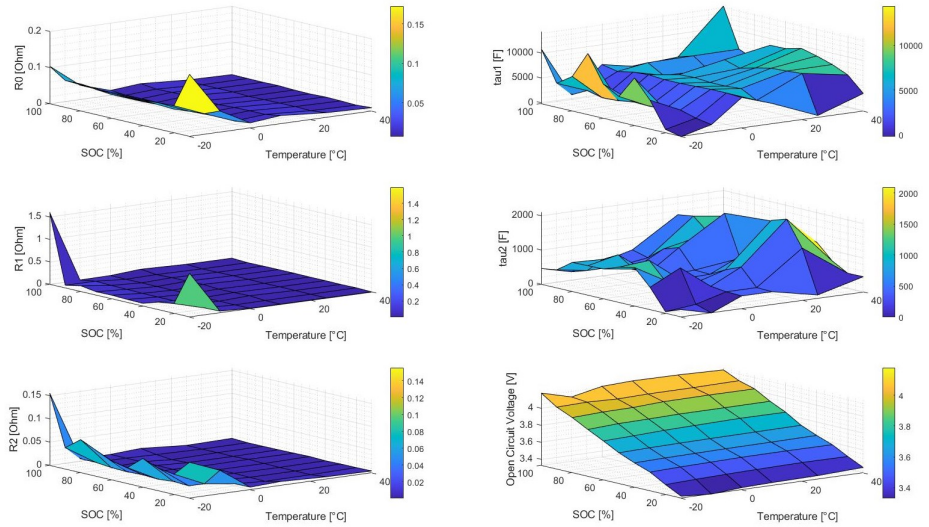

Figure 33. 2D look up tables

4.1.1 Parameter Identification Results

The parameter identification code has worked on all HPPC tests so that 2D look up tables (10 SOC level by 6 temperature) for each parameter of ECM have been generated and implemented in the Simulink model (Table 5, Table 6, Table 7, Table 8, Table 9, Table 10). A self-explaining representation of the 2D look up tables is the surface representation, as

the one from figure 34 to figure 39.
Although all parameters assume meaningless values at 0.1% SOC probably due to bad optimization at really low values of state of charge, this has not been considered as a concern because such low SOC values are never reached in the normal working conditions of a battery.

R0 [Ohm]	-20°C	-10°C	0°C	10°C	25°C	40°C
10 %	0.1726	0.0593	0.0147	0.0233	0.0135	0.0099
20 %	0.0754	0.0417	0.0094	0.0162	0.0089	0.0069
30 %	0.0734	0.0384	0.0109	0.0163	0.0102	0.0084
40 %	0.0701	0.0344	0.0103	0.0152	0.0097	0.0092
50 %	0.0671	0.0366	0.0097	0.0133	0.0090	0.0075
60 %	0.0656	0.0347	0.0088	0.0132	0.0081	0.0080
70 %	0.0694	0.0375	0.0105	0.0166	0.0100	0.0099
80 %	0.0746	0.0373	0.0103	0.0164	0.0099	0.0091
90 %	0.0743	0.0390	0.0101	0.0151	0.0095	0.0094
100 %	0.1035	0.0392	0.0130	0.0200	0.0122	0.0100

Table 5. R0 2D look up table

R1 [Ohm]	-20°C	-10°C	0°C	10°C	25°C	40°C
10 %	0.9772	0.0409	0.0101	0.0087	0.0071	0.0002
20 %	0.2209	0.0318	0.0050	0.0078	0.0081	0.0104
30 %	0.1713	0.0311	0.0061	0.0340	0.0097	0.0043
40 %	0.0631	0.0299	0.0058	0.0229	0.0099	0.0077
50 %	0.0689	0.0297	0.0058	0.0186	0.0063	0.0062
60 %	0.0824	0.0299	0.0058	0.0424	0.0141	0.0098
70 %	0.0764	0.0389	0.0064	0.0339	0.0136	0.0086
80 %	0.1289	0.0436	0.0065	0.0285	0.0084	0.0061
90 %	0.0591	0.0552	0.0055	0.0162	0.0019	0.0008
100 %	1.5997	0.0022	0.0071	0.0542	0.0236	0.0190

Table 6. R1 2D look up table

R2 [Ohm]	-20°C	-10°C	0°C	10°C	25°C	40°C
10 %	0.0776	0.0512	0.0058	0.0089	0.0053	0.0043
20 %	0.0441	0.0143	0.0052	0.0014	0.0019	0.0036
30 %	0.0488	0.0020	0.0048	0.0021	0.0020	0.0035
40 %	0.0622	0.0036	0.0048	0.0028	0.0019	0.0026
50 %	0.0344	0.0005	0.0048	0.0028	0.0023	0.0038
60 %	0.0408	0.0023	0.0048	0.0027	0.0035	0.0030
70 %	0.0556	0.0008	0.0051	0.0020	0.0018	0.0024
80 %	0.0710	0.0019	0.0051	0.0006	0.0020	0.0020
90 %	0.0456	0.0051	0.0050	0.0037	0.0018	0.0018
100 %	0.1555	0.0050	0.0052	0.0090	0.0019	0.0034

Table 7. R2 2D look up table

τ_1 [F]	-20°C	-10°C	0°C	10°C	25°C	40°C
10 %	-170.91	1394.8	6002.5	3952.3	254.83	3411.9
20 %	536.96	1959.9	6179.8	3837.8	7981.3	6412.0
30 %	5693.3	2867.2	6179.2	5479.4	7726.9	7767.0
40 %	9411.8	2279.7	6023.7	5224.5	7556.9	8745.7
50 %	4958.8	2136.7	5927.5	5228.9	6875.9	9542.4
60 %	6698.0	2266.3	5913.9	5480.5	6072.1	8749.0
70 %	12127.9	1772.0	6160.5	5328.9	7042.4	8680.5
80 %	6765.2	1589.7	5932.4	4436.2	4146.3	5097.0
90 %	4641.1	2331.3	5347.9	6258.7	6358.1	6420.1
100 %	10842.5	748.47	5991.9	4789.4	5376.6	14362.4

Table 8. τ_1 2D look up table

τ_2 [F]	-20°C	-10°C	0°C	10°C	25°C	40°C
10 %	219.25	-2.4081	372.80	371.85	93.222	442.02
20 %	49.129	143.35	386.27	386.66	1356.7	436.88
30 %	657.97	1100.6	440.54	880.82	2097.1	689.70
40 %	1129.4	630.56	432.43	694.42	1952.0	1131.5
50 %	1032.4	1105.4	433.87	455.67	1072.3	556.76
60 %	870.65	745.19	430.17	470.34	630.45	800.02
70 %	859.94	1057.8	406.59	1022.5	1840.9	1436.8
80 %	849.98	816.77	396.89	874.17	1149.1	972.56
90 %	525.85	382.23	384.51	510.81	1541.8	1358.6
100 %	457.69	238.16	410.05	634.78	1478.4	999.89

Table 9. τ_2 2D look up table

OCV [V]	-20°C	-10°C	0°C	10°C	25°C	40°C
10 %	3.3553	3.3305	3.3572	3.3665	3.3740	3.3950
20 %	3.4484	3.4615	3.4712	3.4774	3.4849	3.4814
30 %	3.5525	3.5630	3.5699	3.5767	3.5785	3.5765
40 %	3.6176	3.6255	3.6302	3.6348	3.6378	3.6423
50 %	3.6931	3.7016	3.7071	3.7108	3.7146	3.7183
60 %	3.7892	3.8001	3.8141	3.8216	3.8315	3.8289
70 %	3.8806	3.8994	3.9045	3.9125	3.9128	3.9142
80 %	3.9772	3.9930	3.9965	4.0148	4.0186	4.0170
90 %	4.0567	4.0660	4.0538	4.0623	4.0630	4.0697
100 %	4.1788	4.0837	4.1585	4.1733	4.1685	4.1531

Table 10. OCV 2D look up table

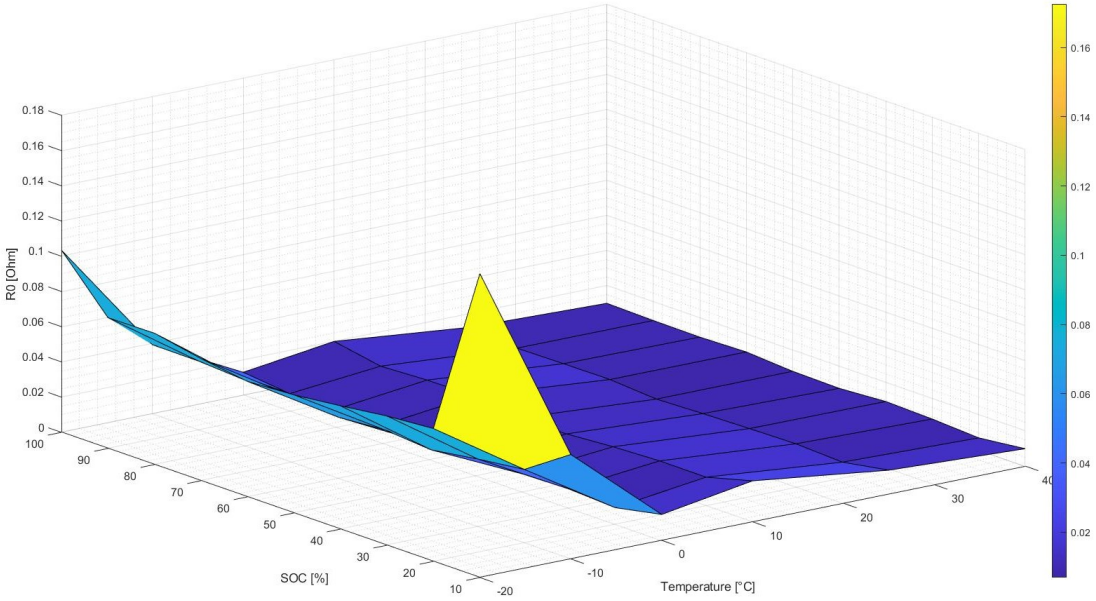

Figure 34. R0 Look Up Table

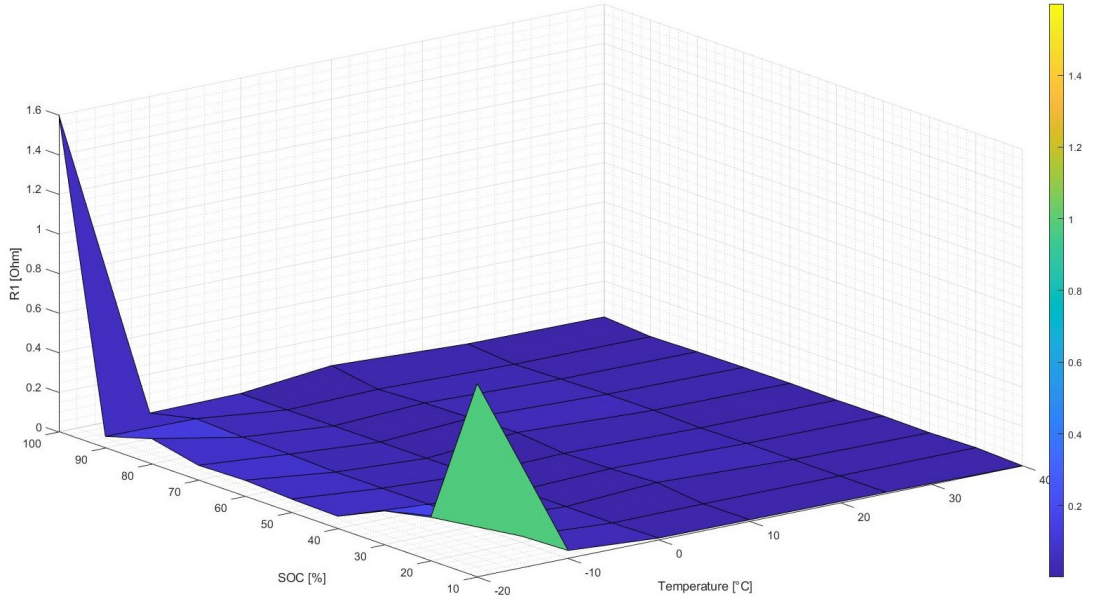

Figure 35. R1 Look Up Table

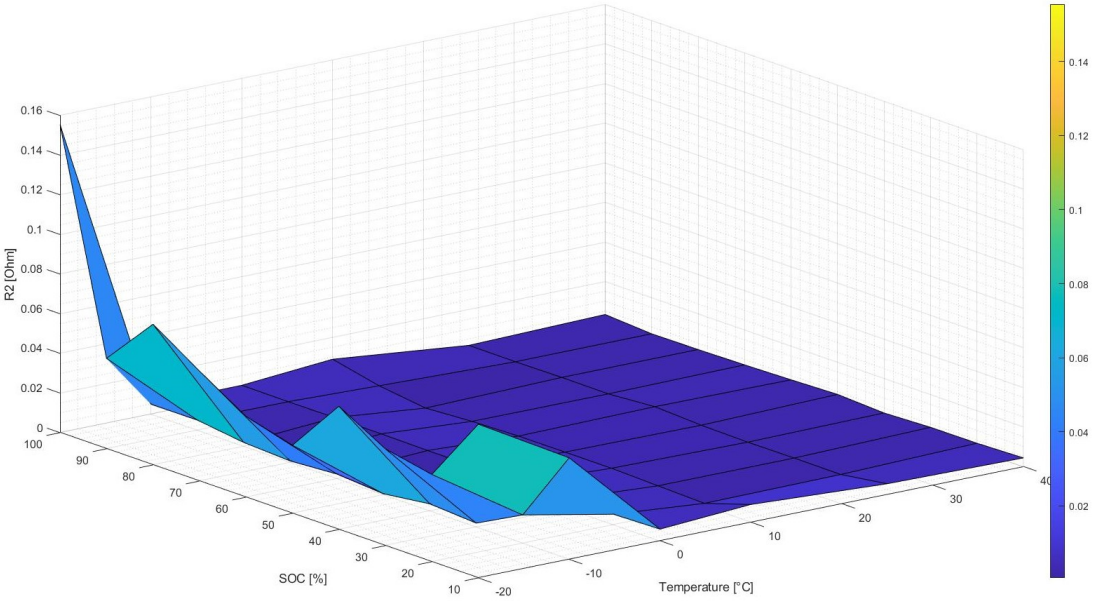

Figure 36. R2 Look Up Table

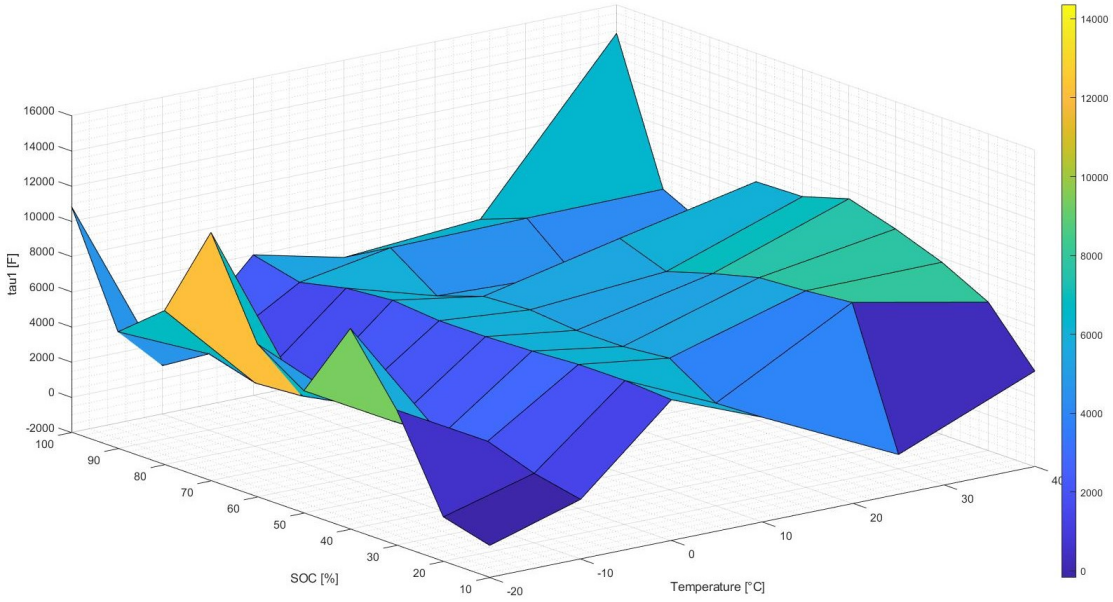

Figure 37. τ_1 Look Up Table

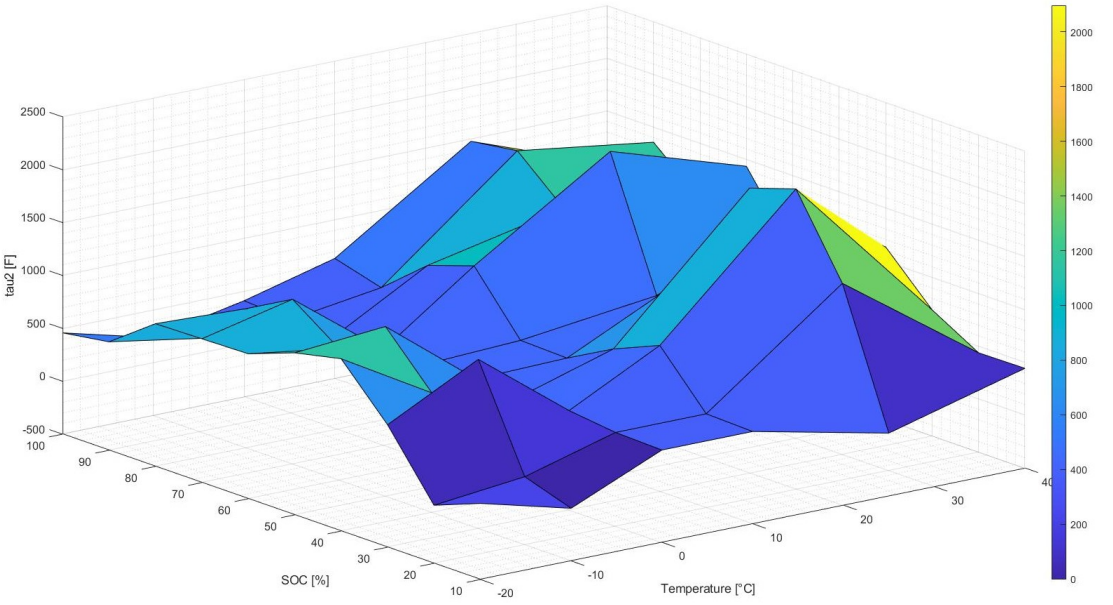

Figure 38. τ_2 Look Up Table

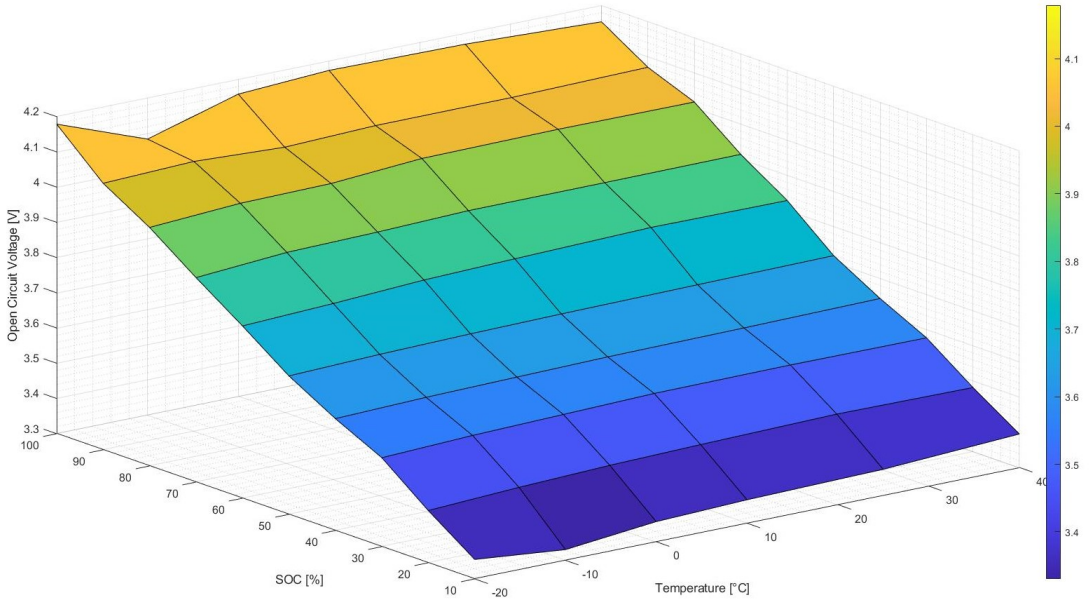

Figure 39. OCV Look Up Table

An useful representation of ECM parameters is the one plotting them as function of state of charge, because, from this view, both the dependency on temperature and state of charge can be highlighted, as shown in figure 40 and figure 41.
For this reason, usually, plots characterizing the parameters of a battery equivalent circuit report ECM parameter as function of SOC.
As can be seen in figure 40, the resistances appear almost linear along the SOC range and slightly varying with temperature, a part from the extremities, whose higher values are probably due to the fact that too high initialization values of the optimization procedure have been imposed.
In particular the highest values concerns R0 resistance probably because it gives the strongest contribution to the overall equivalent circuit model since it models the voltage drop of the battery once it is connected to a certain electrical load.
However, overall resistances values have shown to be compatible with results coming from other studies because of their similar order of magnitude ($m\Omega$) and trend [4].
Instead for what concerns the two τ_1 and τ_2 parameters, in figure 41, it can be noticed their stronger dependency on the temperature.
This could be due to the fact that, since they represent the dynamic behaviour of the chemical processes that are occurring inside the battery, and because chemical reactions are strongly influenced by the temperature, then also these parameters show a tight dependency on the temperature.
To conclude, the linear trend of the open circuit voltage with respect the state of charge, highlighted in figure 41, shows its bigger dependence on the state of charge rather than the temperature whose variation seems to not affect as much its value, as expected.

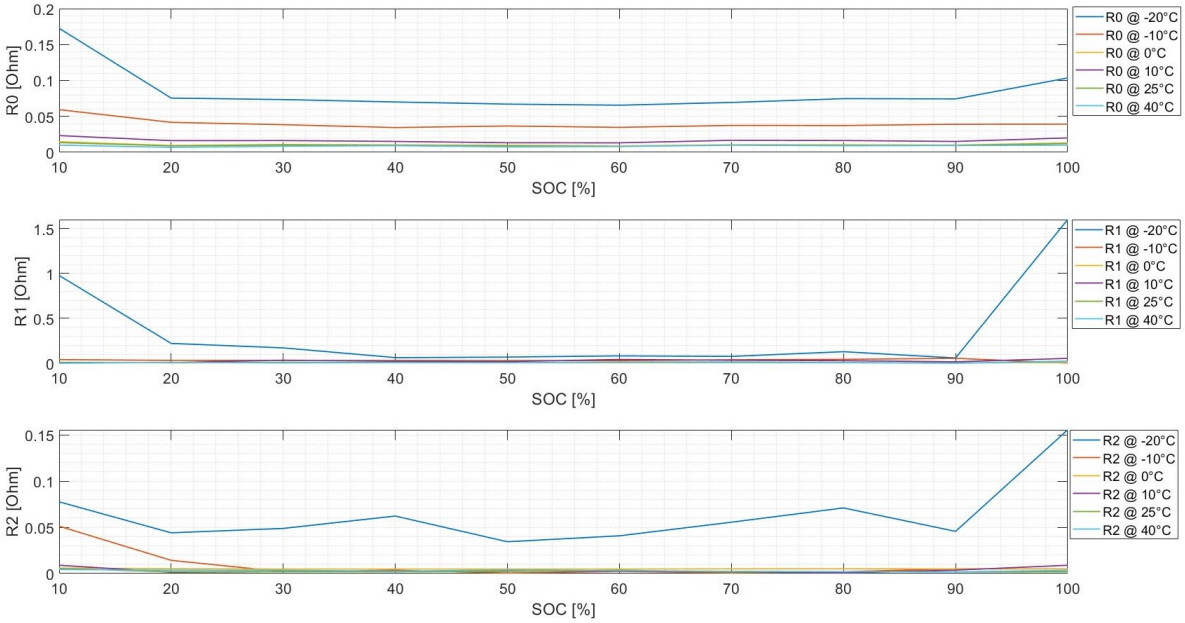

Figure 40. Optimized ECM Resistance values

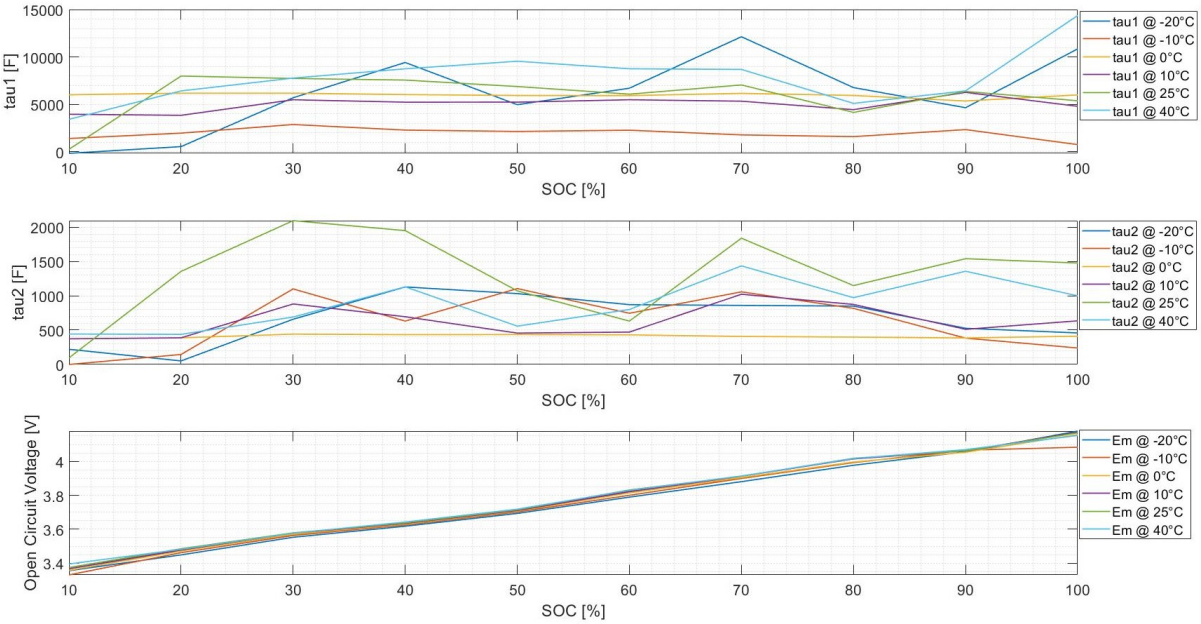

Figure 41. Optimized ECM values

To confirm the validity of these results, two statistical indexes have been employed.
The first is the root mean square error (RMSE, table 11), between the experimental measured voltage signal and the simulated signal coming from the model implemented with the optimized parameters.

$$RMSE = \sqrt{\frac{1}{N}\Sigma_{n=1}^{N}|V_{tgt} - V_{sim}|^2}$$

Together with RMSE, also the maximum absolute error among the two voltage signals has been reported.
Residuals have been considered as second validation index: a residual is the difference between the observed value and the estimated value of the quantity of interest, in this case referring to the measured and the modelled voltage signal.
From figure 43 to figure 46, both of these indexes have been reported for all the temperature cases.

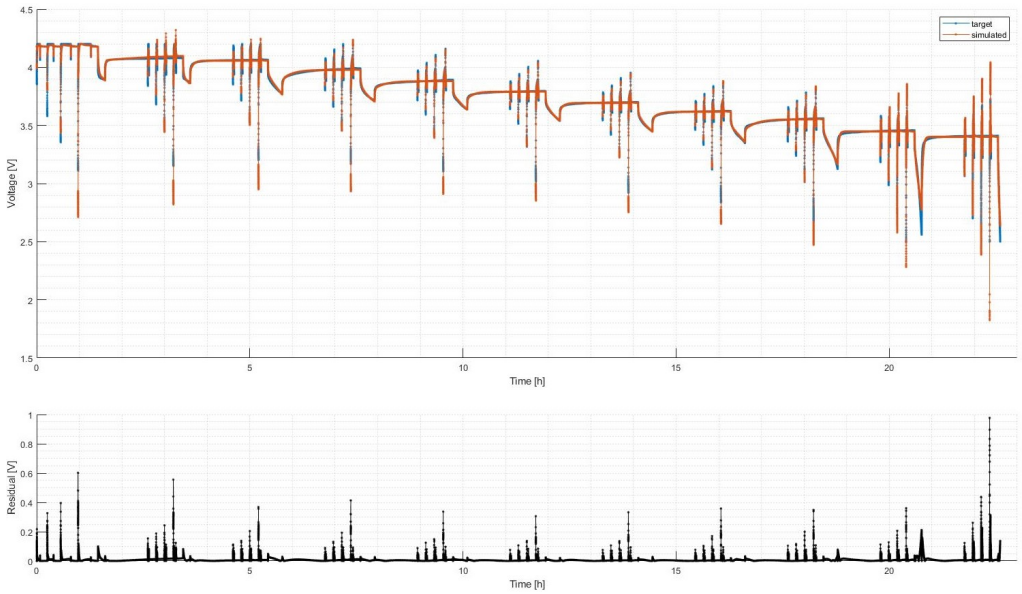

Figure 42. Voltages and Residuals at -20°C

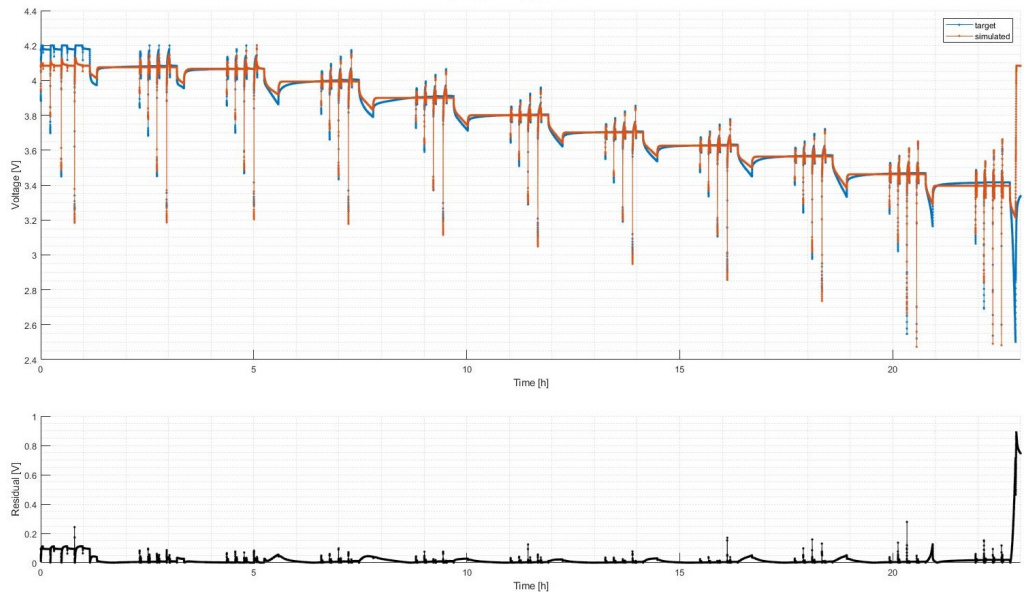

Figure 43. Voltages and Residuals at -10°C

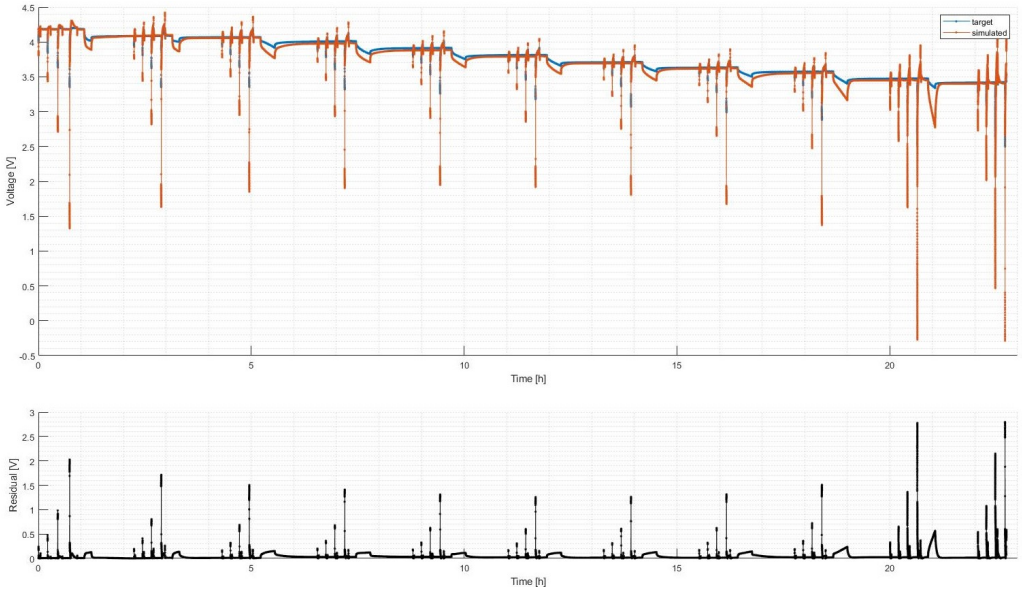

Figure 44. Voltages and Residuals at 0°C

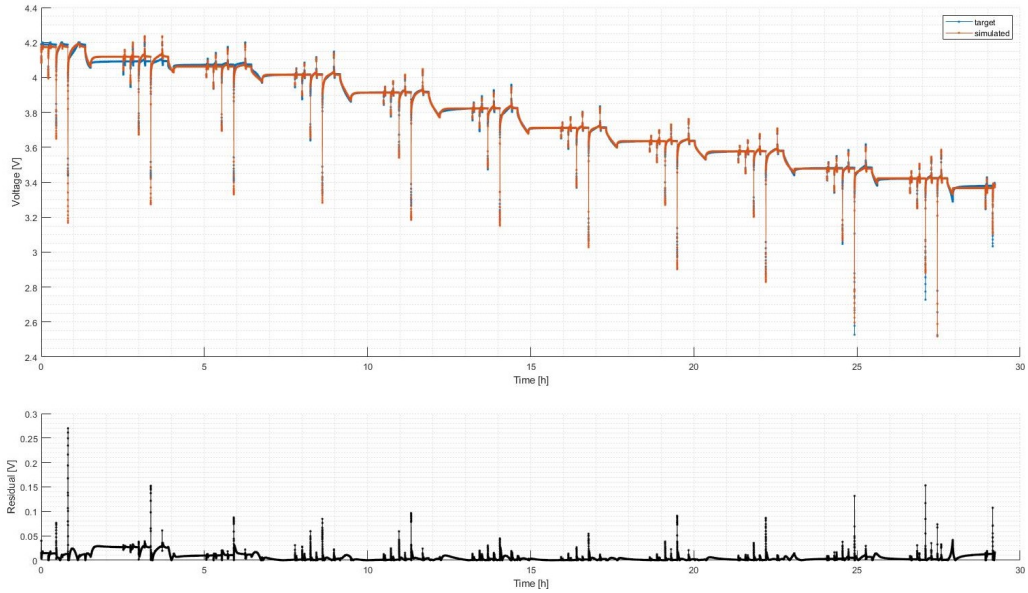

Figure 45. Voltages and Residuals at 10°C

As it can be noticed, the lower are the residuals, RMSE and maximum absolute error, the more accurate is the estimation of the model with respect the original experimental signal. It means that the optimization procedure of parameter identification has provided significant results.

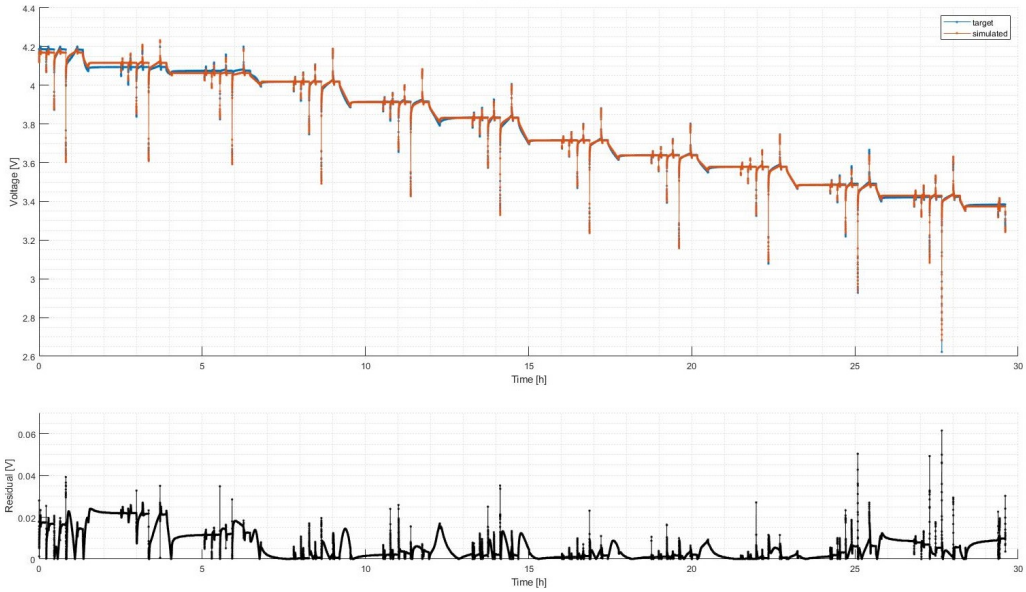

Figure 46. Voltages and Residuals at 25°C

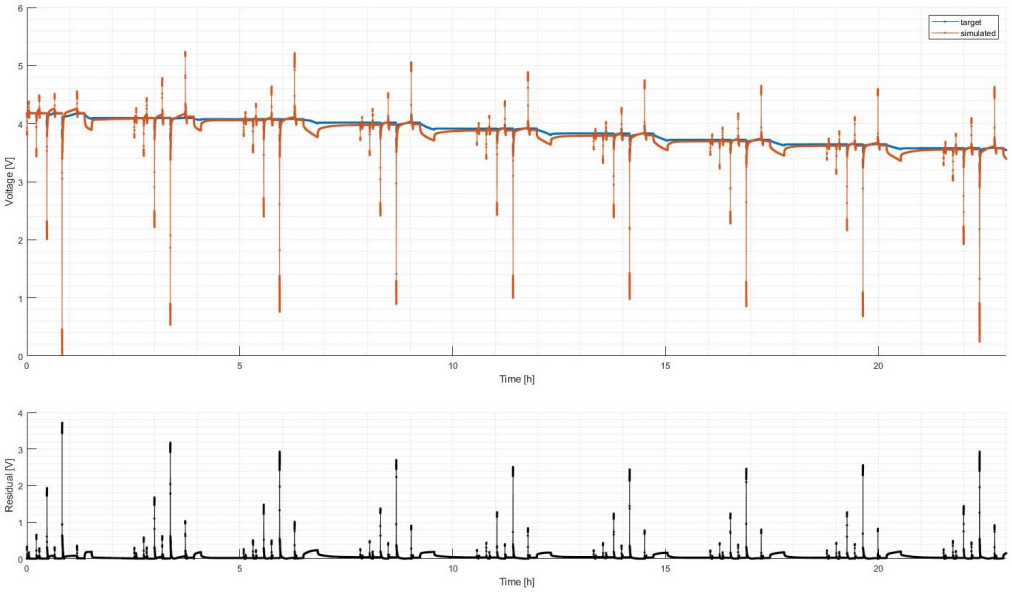

Figure 47. Voltages and Residuals at 40°C

T [°C]	-20	-10	0	10	25	40
RMSE [-]	0.017506	0.30868	0.092978	0.01044	0.0089355	0.14024
MAX ABS ERR [-]	0.97697	0.89025	2.7967	0.26993	0.061467	6.1007

Table 11. RMSE, Maximum Absolute Error, Voltage

As shown in figure 43, experimental and simulated voltages from HPPC data at -10°C are almost coinciding during the discharging phase, while at the end of the simulation they differ because the model has not been suited for the charging of the battery.
For this reason, during the evaluation of temperature results in the next section, the end

of the simulation has been voluntary cut off, since battery model is not working correctly under the charging phase.
In figure 48, the last of this section, it can be seen that the trends of output voltage, both modelled and simulated, the input current representing the HPPC cycle and the state of charge of the battery, show a coherent behaviour.
For instance peaks in the voltage signal are present where peaks in the current profile occur, as well as small charge peaks are responsible for the little increase in the state of charge.
Also peaks in temperature plot have occurred at the same time of the highest discharge current pulses during the HPPC cycle.
This means that the overall model, from what concerns both the electrical and thermal part, has worked in a proper way.

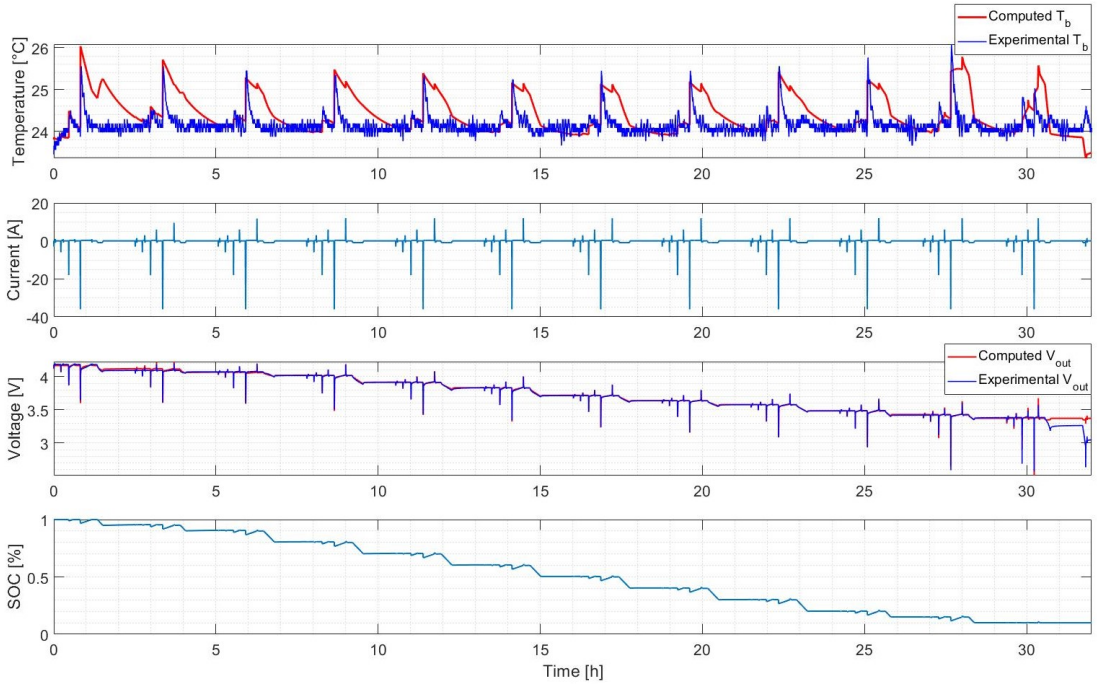

Figure 48. Simulink Battery Model Results at 25°C

4.1.2 Thermal Model Results

In this section, the outcomes of the thermal model will be exposed.
The plots from figure 49 to figure 54 represent the modelled temperature of the cell and the experimental one (blue line) as function of time in two cases: the one considering the entropic contribution (black line) in the heat generation of the cell, also called reversible heat, and the other without considering it (red line), i.e. just with irreversible heat.
This has been done to assess its influence on the overall battery behaviour, since it has usually been neglected in other studies from the past.
Furthermore, being this a subtracting contribution to the generated heat inside the battery,

it has helped to lower the value of heat transfer coefficient, thus closer to a more realistic value satisfying the natural convection.
All the results have been reported by taking certain values of heat transfer coefficient and specific heat of the battery:

$$h = 7.5\ [\frac{W}{m^2 K}]$$

$$c_{p,b} = 1800\ [\frac{J}{kgK}]$$

As already explained in chapter 1, h has been chosen to respect the natural convection air cooling, while c_p has been chosen according to the outcome from a procedure utilizing the parameter estimation tool in Matlab, whose goal has been set to correctly match the experimental results with the modelled one.

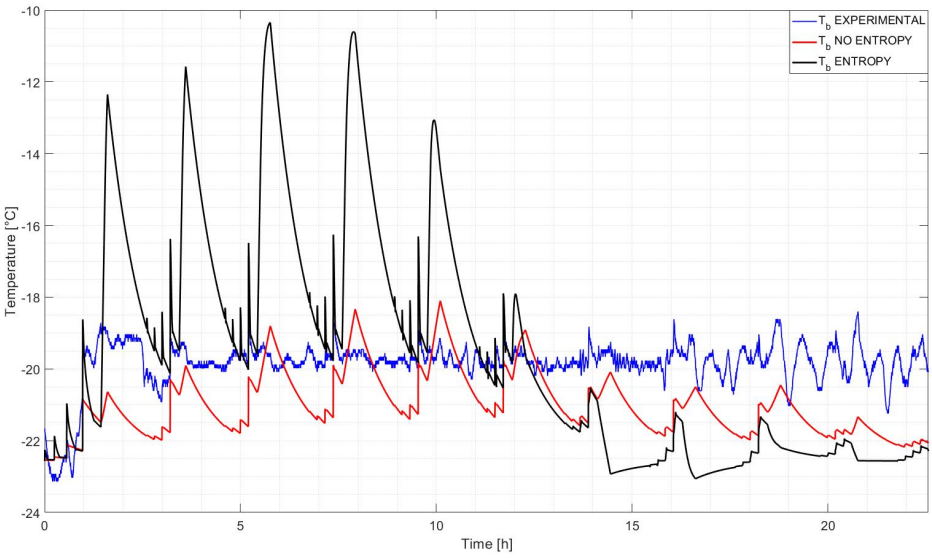

Figure 49. Tb vs experimental Tb at -20°C

Starting from figure 49, it can be noticed that, in the case without entropic contribution, the overall experimental profile has almost been followed by the simulated temperature, even if with some errors.
The cause lay in the fact that, at such lower temperatures, all the properties of the battery change a lot due to their higher sensitivity, and should be investigated each one with apposite experimental procedures.
Also the experimental data shows big oscillations, meaning that battery behaviour in such extreme conditions is really unpredictable.
Anyway, this is a common problem in the development of battery models and an appropriate calibration at these temperatures is to be investigated more in depth.

The second case with entropic contribution shows inconsistent results, probably due to the choice of computing the entropic coefficient with a simplified incremental ratio whose data are extrapolated by the 2D look up table.
At -10°C, both plots of simulated temperatures with and without entropic contribution (Fig. 50) show a more regular profile and a better fitting of the data extracted from experiments. For the same reason of the previous data-set, at such low temperature, battery behaviour is unstable and so the huge oscillations at the end of the test are explained.
Furthermore, it can be noticed that, considering the reversible heat, the simulated profile is better matching the experimental temperature profile, even if with some discrepancies for what concerns the initial temperature peaks.
In both cases the model overestimates the temperature of the cell, but in the one without entropy it can be seen that also the cooling of the battery in between the temperature peaks shows a slower behaviour, since the modelled temperature decreases in a slower way.
This could have happened for two reasons: the first is that the specific heat of the battery could have been set too high, meaning an higher capability of the battery to hold the heat, thus slowing the cooling. Instead the second concerns the convective heat transfer coefficient, that could have been set too low thus avoiding a proper convective cooling of the cell by the air.
The problem in the latter case is that an higher h would have meant also a forced cooling, which is not the case of the experiment.
However, the simulated temperature considering reversible heat, has shown a better fitting at the same values of h and c_p rather than the other model where just irreversible heat contribution has been implemented.

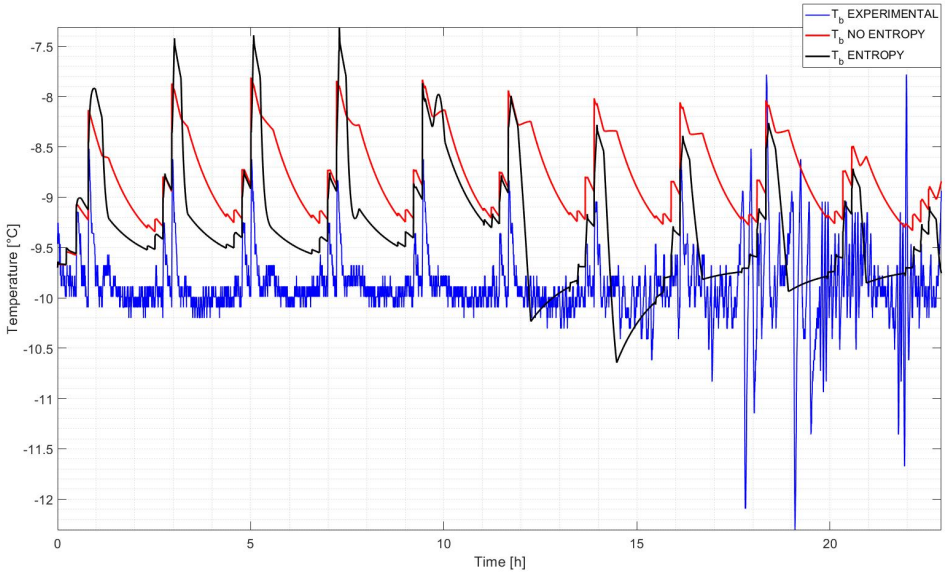

Figure 50. Tb vs experimental Tb at -10°C

In the 0°C temperature range, results are similar , if not better, to the previous results just analysed and the considerations are the same, except for one aspect concerning the model with reversible heat (figure 51): in this case the starting peaks of modelled temperature are totally inconsistent.
This probably because of close to zero values of temperatures that could have generated some troubles in the computation of the entropic term at the beginning of the simulation.

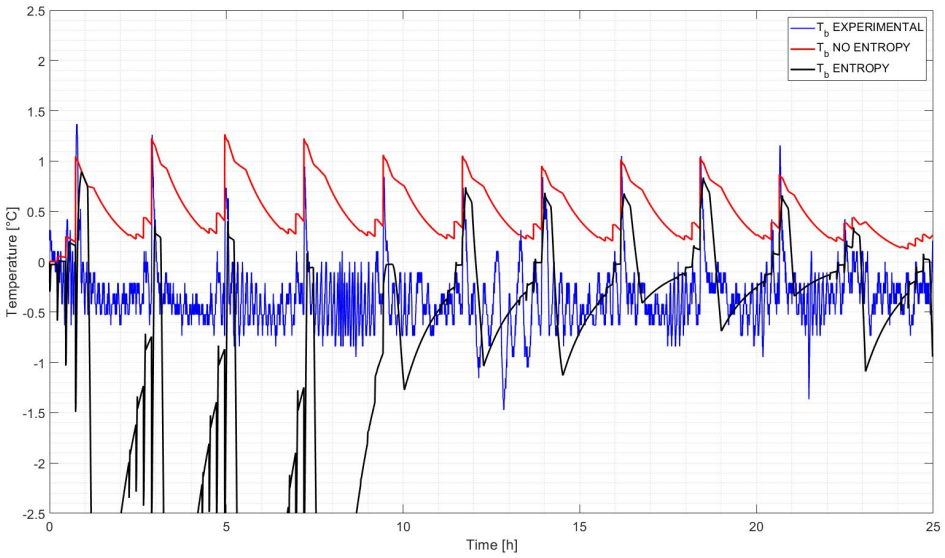

Figure 51. Tb vs experimental Tb at 0°C

From figure 52 to figure 54, issues related to cold temperatures are not present anymore; this is confirmed by the fact that experimental temperature profiles (blue lines) are regular without any huge oscillation, a part from the smaller ones due to the acquisition sampling noise.
As a general consideration, all the plots of simulated temperature considering the reversible heat, show a better fitting of experimental measures both for what concerns the various peaks, that are almost always coinciding, and the thermal inertia of the battery, which seems to have an higher cooling capability, or be simply lower, since temperature plot have a steeper slope after each peak.
Instead, in the plots where the model is embedded just with the irreversible heat generation due to Joule Effect, it can be noticed that all the simulated temperatures overcome the experimental one sightly more than the other model, both in the peaks of temperature and in the transient cooling behaviour, being the trend with a lower steepness, meaning a slower cooling capability or an higher heat retention.

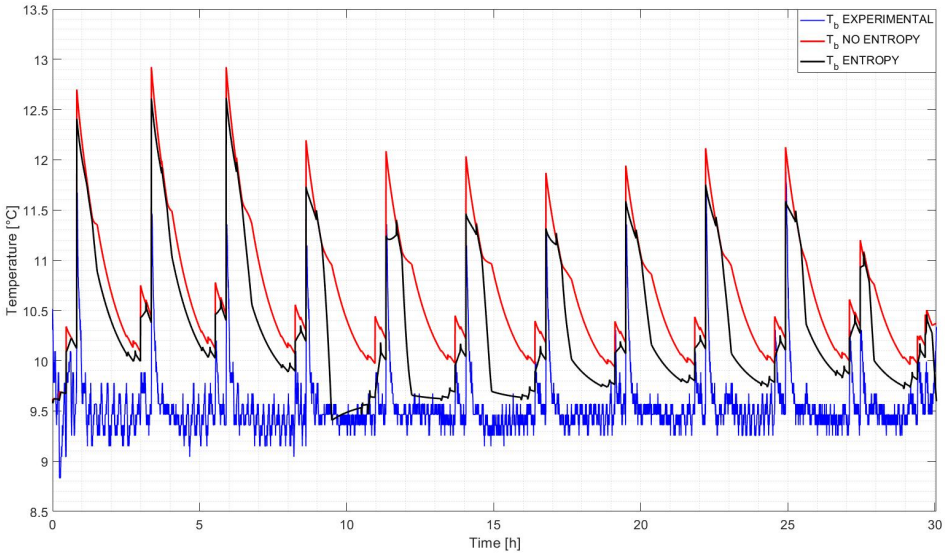

Figure 52. Tb vs experimental Tb at 10°C

A weird behaviour, noticeable in all the plots considering reversible heat, is the second smaller temperature peak after the first one.
The reason could lie in the fact that computation of the entropic term throughout the incremental ratio, exploiting the 2D look up tables, is not perfect but it magnifies the little discontinuities present also in the plots of the model without entropic contribution.
Although in the 25°C results of figure 53, it can be noticed that in some points, the model underestimates some peaks of temperature, being these really sporadic and in the order of less than half Celsius Degree, it has not been regarded as a relevant issue.

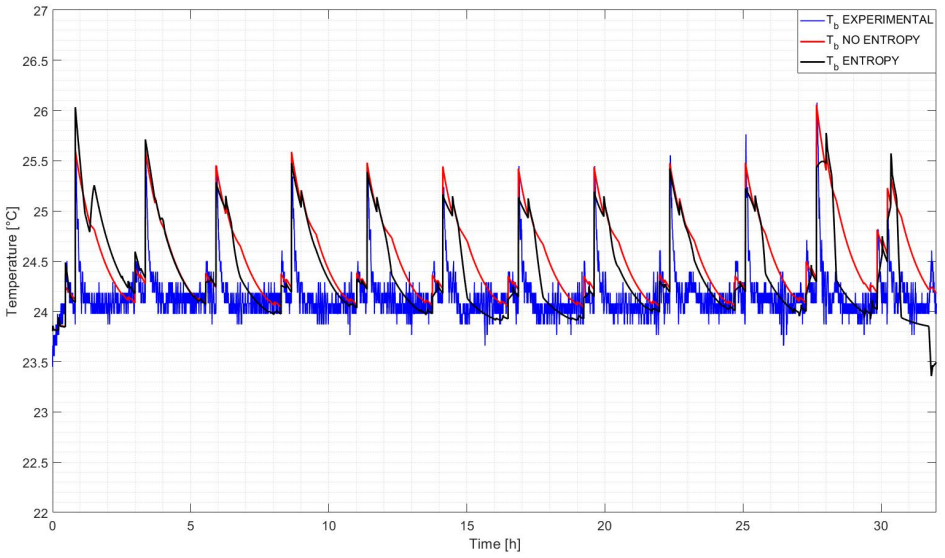

Figure 53. Tb vs experimental Tb at 25°C

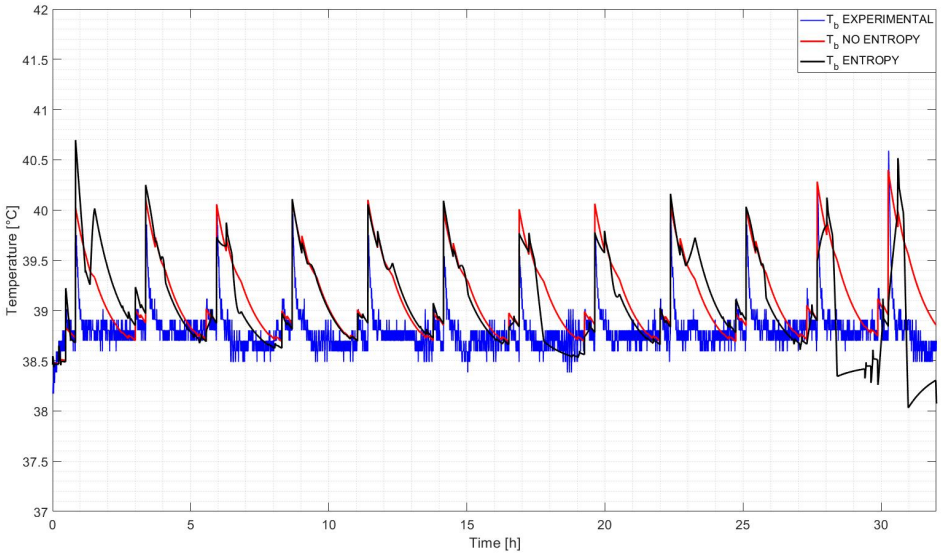

Figure 54. Tb vs experimental Tb at 40°C

Root mean squared value between the modeled and measured temperature has been chosen as parameter in order to perform a statistical analysis and to assess the accuracy of the results.

$$RMSE = \sqrt{\frac{1}{N}\Sigma_{n=1}^{N}|T_b - expT_b|^2}$$

As highlighted in Table 12, for higher temperatures, results have showed a lower RMSE and so a better accuracy of the model.
Considering the entropic term in the heat generation has led to weird temperature profile in the case of 0°C, thus resulting in higher RMSE values.
The same has happened in the cases of colder temperatures as -20°C and -10°C where RMSE values are higher due to some bad oscillations in their temperature profiles at the beginning of the simulation, even if at the end, results have almost followed the experimental temperature data.

T [°C]	-20	-10	0	10	25	40
RMSE_ENTR [-]	3.1130	0.8015	1.9006	0.9671	0.4619	0.5015
RMSE_NO_ENTR [-]	1.4471	1.1655	0.9003	1.2369	0.5067	0.4650

Table 12. RMSE Temperature

4.2 Battery Rack Results

In this section, temperatures coming from the battery model developed in the Simscape environment will be reported.

The first part concerns the comparison among Simulink and Simscape results.

The single row made out of five cells is analysed in the second part of this section.

Finally results coming from the battery rack model made out of 25 cells arranged into 5 rows, are reported in the last part.

4.2.1 Single Cell Models Comparison

Before to start the development of the overall battery model in the Simscape environment, it has been necessary to assess if this methodology of work had provided the same results as the Simulink model for the single cell, where calibration of some key parameters has been done, as explained in chapter 2.
The comparison among these two methodologies of work has been carried also to further confirm the validity of the Simulink model.
Results refer to the single cell model without considering the reversible heat inside the heat generation, since there have been some issues in implementing that contribution in the Simscape model.

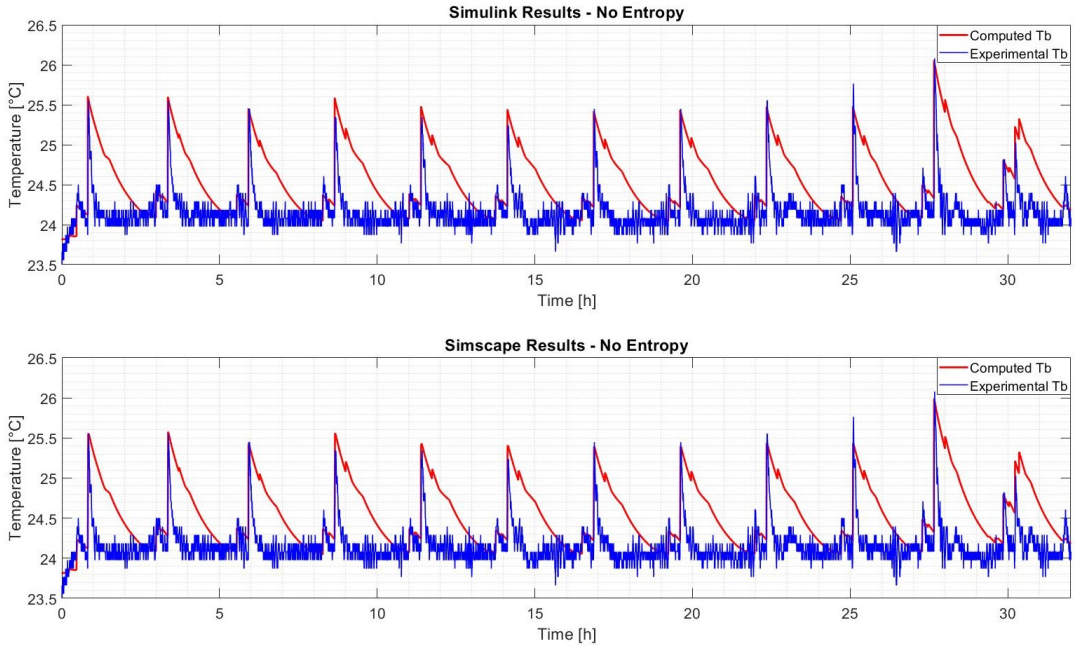

Figure 55. Comparison Simscape - Simulink Single Cell Model, No Entropy

As shown in figure 55, it can be noticed that temperature profiles coming from the two models perfectly match each other, meaning that also adopting the Simscape methodology is a correct way to develop a battery model, instead of the purely numerical Simulink one.

4.2.2 5 Cells Row Model

Once the choice to proceed with the Simscape methodology has been taken, the single row model made out of 5 cells have been developed.
Three models have been developed to analyse the behaviour of the battery in case of different heat exchanges.
The only assumption in this phase is that the row is isolated from the environment in the upper and lower side, while convective heat exchange with it occurs only through the first and last cell of the row.
The first model (Fig. 56) has been embedded with only convective heat transfer blocks in between the cells of the row, differently from the second one (Fig. 58), where only conduction blocks among them have been adopted.
In the last model (Fig. 60) a series of conduction and convective blocks have been implemented, to analyse all the possibilities.

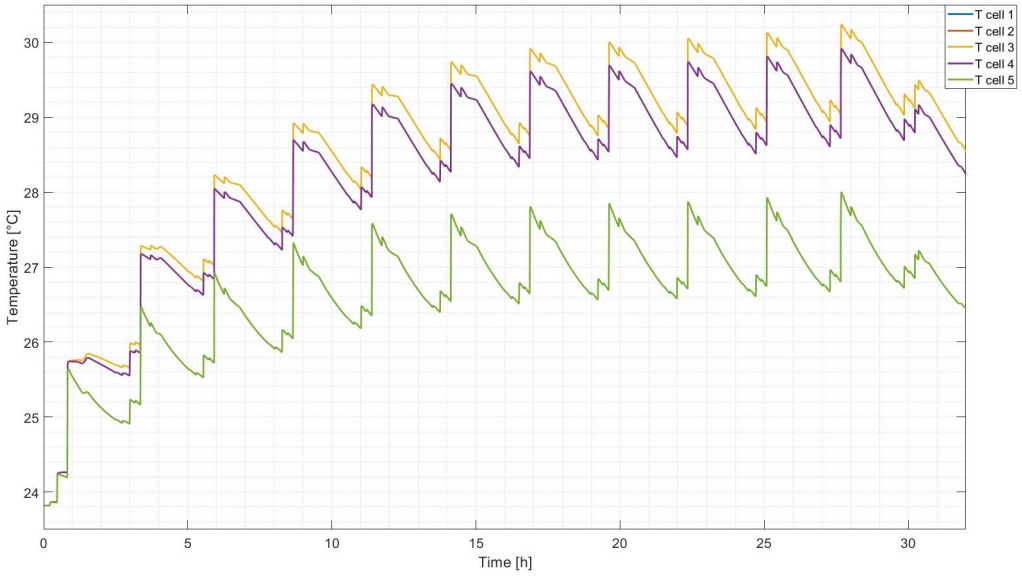

Figure 56. Simscape Row Model, Convection

As shown in figure 56, the overall temperature trend is increasing while the battery is undergoing the HPPC cycle, as expected.
The symmetric behaviour of the cells is also another confirmation of the fact that the results are truly representative of what would happen in reality: the third cell in the middle, is the

one heating the most, while cells 2 and 4 are heating slightly less but in the same way. The end cells 1 and 5 instead are heating much less due to the fact they are cooled by ambient air because of the convective heat transfer blocks implemented in the model.
Since temperature trends of cell 2 and 4 and the one of cell 1 and 5 are superimposed because of the symmetry of the row, figure 57 shows the trend of cell 1 and 2 that exactly match the trend of cell 5 and 4 respectively.

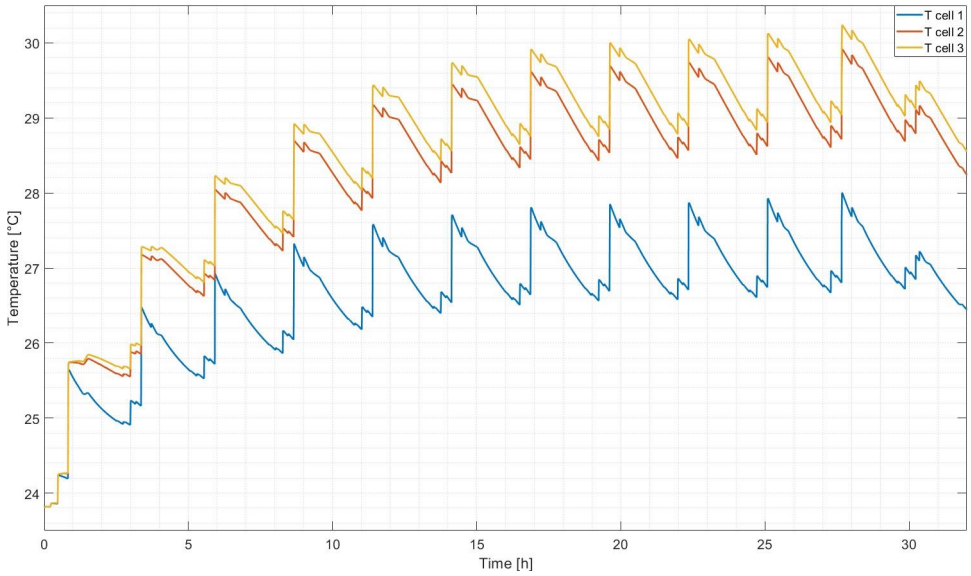

Figure 57. Simscape Row Model, Convection 1-3

For what concerns the model embedded with just conductive heat transfer blocks, it can be noticed in figure 58 that differences of temperature among cells is less pronounced, probably due to the fact that conduction is occurring among cylindrical surfaces, that have in theory only one contact line, the tangent one.
Reducing the heat transfer surface, also the exchanged heat amount will be lower and so the heating of the cell.
Furthermore, also the isotropic thermal conductivity considered in this dissertation, could not have had the most correct value, but in absence of experimental data to calibrate it with, the values taken from the literature [14] has been the only possible choice.
Figure 59, shows a zoomed view of a temperature peak of this model, where it can always be seen the symmetric and correct behaviour of the row, where the middle cell is heating the most and the outer cells are heating the lower, with a superimposed behaviour as well as the inside cells 2 and 4.

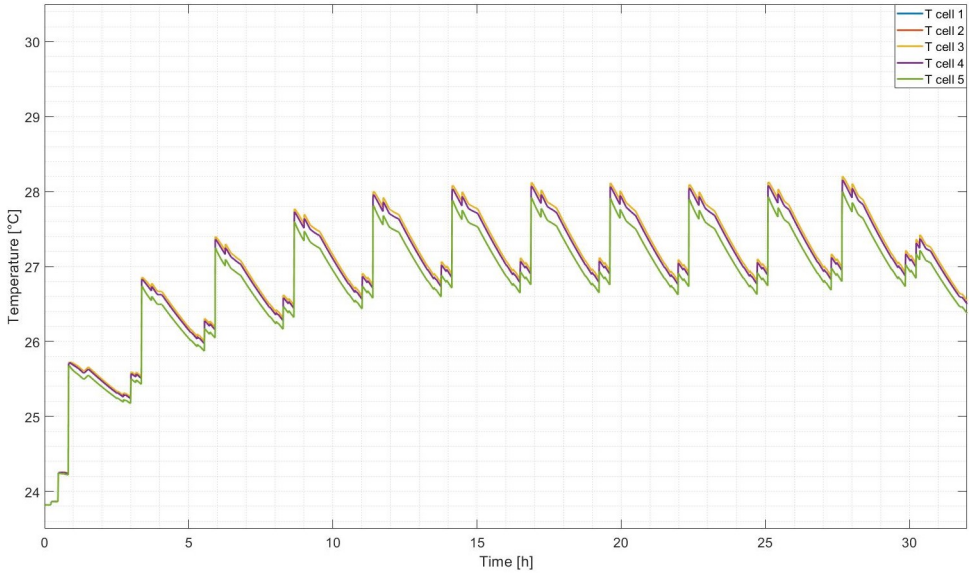

Figure 58. Simscape Row Model, Conduction

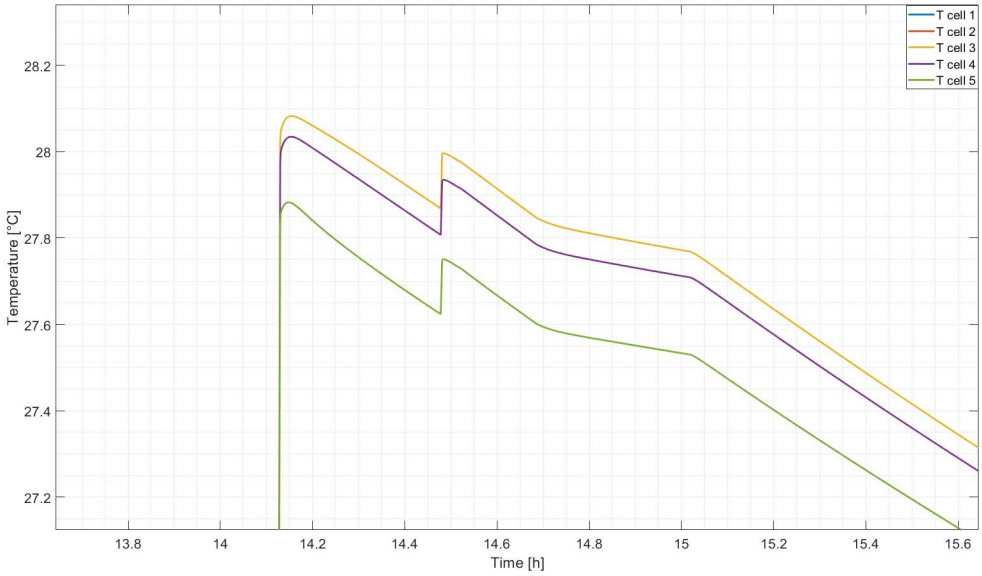

Figure 59. Simscape Row Model, Conduction Zoom

The last figure of this section, figure 60, shows the temperature trends coming from the model with both conduction and convective heat transfer blocks.
Here, it can be noticed a slightly higher overall temperature trend, in accordance to the expectations since both contributions help in generating an higher exchanged heat among the cells.

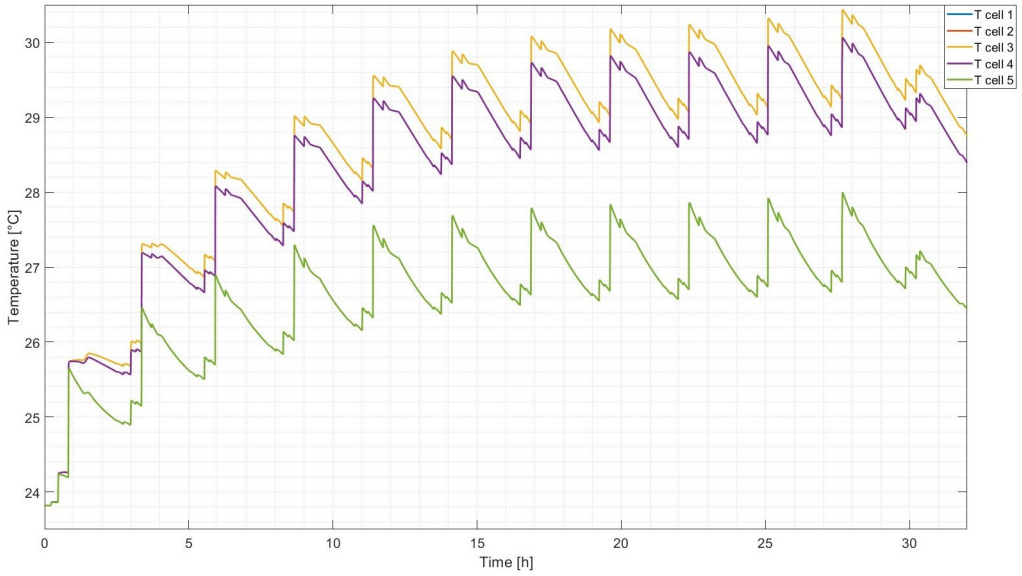

Figure 60. Simscape Row Model, Conduction and Convection

4.2.3 Battery Rack Model

Input current for the battery model is the same HPPC cycle at 25°C coming from literature [1], already utilized for the simulation of the single cell model.
It has been slightly modified in order to highlight the differences among temperature profiles of the different cells, always paying attention to not overcome the maximum discontinuous discharge current of 14.7A of the single cell, as reported in table 2.
In general, in all the presented results, temperature variations are in the order of less than 2°C. This is due to the fact that battery pack is made out of few cells with respect a real battery pack where implemented cells are in the order of hundreds.
The choice of implementing just 25 cells has been taken to reduce the complexity of the model and so the computation time of the simulation.
It has been chosen to split the lateral surface of the cell into 6 parts, corresponding to the dots of figure 30, in order to build two matrices of values representing the heat exchange areas in the case of contact among cell and ambient air, or contact among closer cells.
In case of cells belonging to different rows, heat exchange area has been considered as cells were in contact with the cell of the next row, but without any heat transfer block.
Results of figure 61 and 62, refer to a model only considering convective heat exchanges.
As in the case of the single cell, peaks of temperature occurred once a peak in the HPPC cycle occurs, but in this case, being more cells, the cooling is less effective, and so the overall temperature trend tends to increase.
Temperature profiles of the middle row (cell 11-15) is reaching higher values, in accordance with expectations, since the inside cells have a bigger surface involved in the

heat exchange, thus generating an higher heat, because they are in between other cells belonging to different rows.

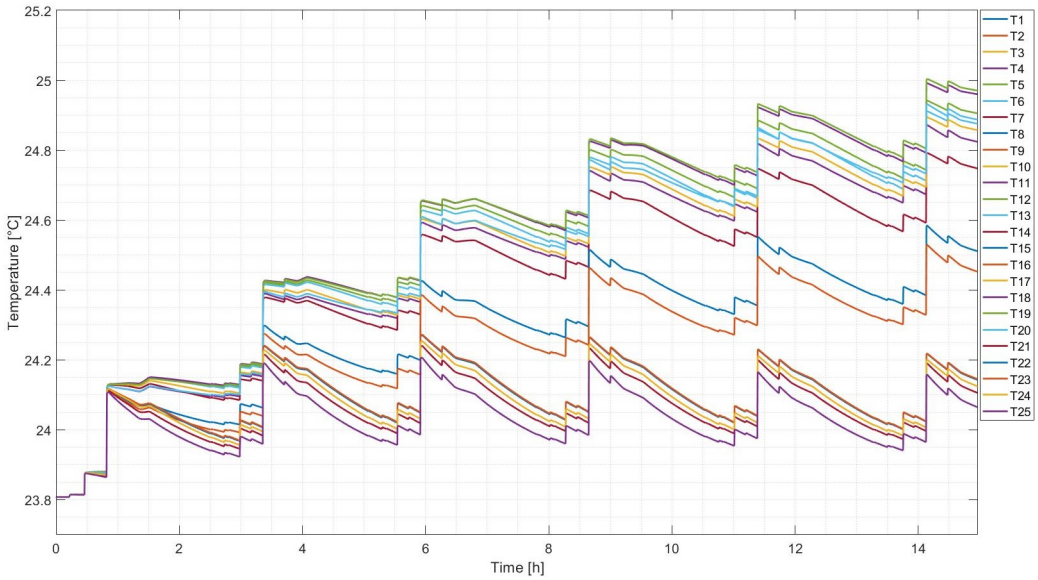

Figure 61. Simscape Model, Convection

In the row plots of figure 62, it can be seen the symmetric behaviour of the second and fourth row, as well as the one of upper and lower rows, as it should be, since they are arranged in the same way.
Outer rows temperatures are reasonably lower than temperatures of inside rows because all of their cells are exchanging heat with the environment, thus being cooled.

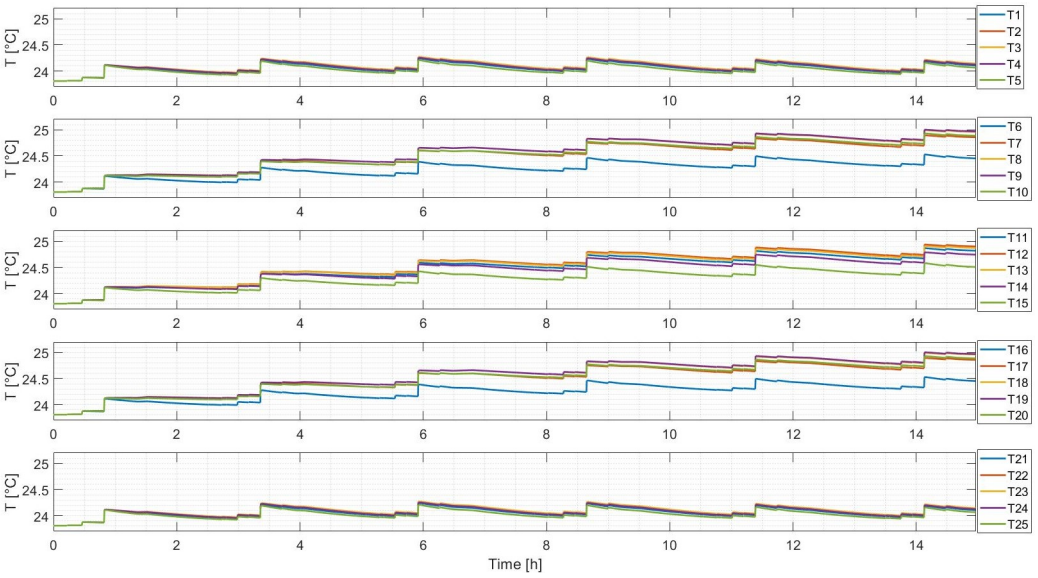

Figure 62. Simscape Model, Convection, Rows

A little difference with respect the single row results is that, being the cells heat exchange areas different, now temperature profiles inside the row are not symmetric anymore. Anyway temperature trend of the cells is coherent with the proposed layout of the battery. For instance in figure 62, temperature of cell 19 is the highest of the row since all of its surface has been considered exchanging heat, as the cell 17, but with the difference that the closer cell cooled by the environment has a smaller involved area in the heat transfer. In this way cell 19 has been heated a little more than cell 17, resulting in a slightly higher temperature.

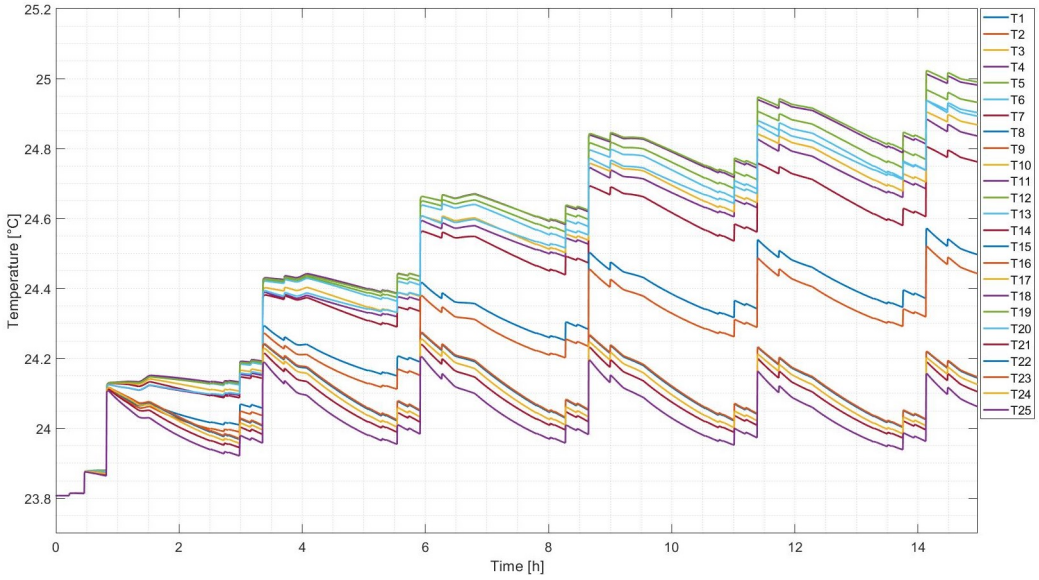

Figure 63. Simscape Model, Convection and Conduction

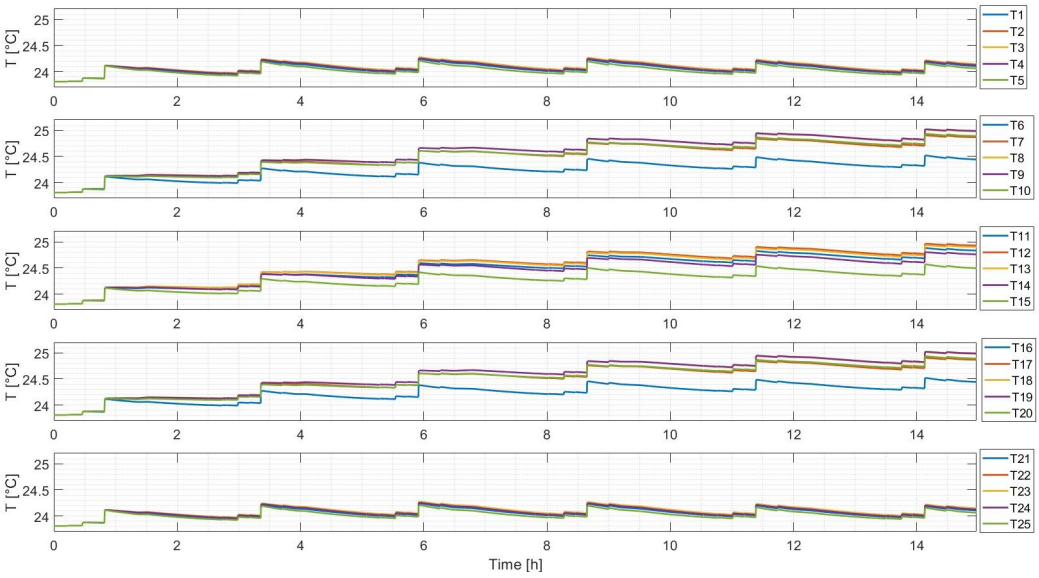

Figure 64. Simscape Model, Convection and Conduction, Row

Regarding the results of figure 63 and 64, where also a small conduction contribution has been implemented, the considerations about the behaviour of various temperature trends are mostly the same.
The only noticeable difference is that temperature peaks have reached slightly higher values than the other model.
This could be for two reasons: the first one is that thermal conductivity could have been underestimated, while the second and most probable one, is that conduction contribution is not so relevant in these kind of models, at least if the battery pack is small as the one analysed throughout this dissertation and as long as cells have a cylindrical shape instead of a prismatic one.

Conclusion

4.3 Conclusion

The aim of this thesis has been to develop a thermal model of a Lithium-Ion battery based on a single temperature lumped parameter model in order to estimate its temperature under dynamic conditions. Firstly, it has been necessary to build an equivalent circuit model of a single cell, with two RC branches to simulate electrochemical behaviour of the battery. The dependency of these parameters on the temperature have been obtained by a procedure of parameters identification, where an optimization based on the comparison with experimental data at different temperatures coming from the literature has been carried out. Simulated tension coming from ECM embedded with optimized parameters at each temperature of -20°C, -10°C, 0°C, 10°C, 25°C and 40°C have matched experimental tension in a proper way, showing low values of RMSE and residuals. Once optimized parameters have been arranged into look up tables and implemented in the model, a thermal model has been developed based on the energy balance equation and on the Bernardi's equation of heat generation. The biggest encountered issue has been related to the reversible generated heat inside the battery due to entropy, anyway, solved by computing it with an incremental ratio, exploiting the look up tables. In this case results have showed that implementing this contribution, the convective heat transfer coefficient and specific heat of the battery have assumed more realistic values of 7,5 $\frac{W}{m^2K}$ and 1800 $\frac{J}{kgK}$ respectively. The simulated temperature profiles have almost always followed the experimental profiles, showing some criticalities only at lower temperatures, where battery behaviour is strongly nonlinear and difficult to predict due to instabilities of the electrochemical species inside it. Once the characterization of the single cell has been completed with all parameters optimized and calibrated, a simpler battery model has been developed in the Simscape environment, whose temperature results have not been validated due to the lack of experimental data but have showed a behaviour in accordance with expectations.

4.4 Future Work

Possible future works will be focused on a more precise calibration of the thermal model coefficients related to a better single cell experimental characterization, as well as a better computation of the entropic term in the heat generation, carrying on a curve fitting procedure. For what concerns the full battery model, it could be built using the single cell Simulink model instead of the Simscape environment, to reduce the computation time of

the simulations. Finally the overall battery model will be further validated and calibrated whenever experimental data coming from test procedures of the physical battery will be available.

References

[1] Phillip Kollmeyer. *Samsung INR21700 30T 3Ah Li-ion Battery Data*. eng. 2020.

[2] Ali Emadi. *Advanced electric drive vehicles / Ali Emadi*. eng. Energy, Power Electronics, and Machines. Boca Raton: CRC Press, 2015. ISBN: 9781466597693.

[3] Jiechao Lv et al. "Estimation of the State of Charge of Lithium Batteries Based on Adaptive Unscented Kalman Filter Algorithm". In: *Electronics* 9.9 (2020). ISSN: 2079-9292. URL: https://www.mdpi.com/2079-9292/9/9/1425.

[4] Martel Tsirinomeny, Hardi Hõimoja, and Alfred Rufer. "Ultrafast Charging Compatibility of Electric Vehicles". In: Mar. 2012.

[5] Edoardo Locorotondo et al. "Online Identification of Thevenin Equivalent Circuit Model Parameters and Estimation State of Charge of Lithium-Ion Batteries". In: *2018 IEEE International Conference on Environment and Electrical Engineering and 2018 IEEE Industrial and Commercial Power Systems Europe (EEEIC / I CPS Europe)*. 2018, pp. 1–6. DOI: 10.1109/EEEIC.2018.8493924.

[6] Edwin Paccha-Herrera et al. "Thermal Modeling Approaches for a LiCoO2 Lithium-ion Battery—A Comparative Study with Experimental Validation". In: *Batteries* 6.3 (2020). ISSN: 2313-0105. DOI: 10.3390/batteries6030040. URL: https://www.mdpi.com/2313-0105/6/3/40.

[7] D. Bernardi, E. Pawlikowski, and J. Newman. "A General Energy Balance for Battery Systems". In: *Journal of The Electrochemical Society* 132.1 (Jan. 1985), pp. 5–12. DOI: 10.1149/1.2113792. URL: https://doi.org/10.1149/1.2113792.

[8] Jiaqiang E et al. "Effects of the different air cooling strategies on cooling performance of a lithium-ion battery module with baffle". In: *Applied Thermal Engineering* 144 (2018), pp. 231–241. ISSN: 1359-4311. DOI: https://doi.org/10.1016/j.applthermaleng.2018.08.064. URL: https://www.sciencedirect.com/science/article/pii/S1359431118330837.

[9] Xiaogang Wu, Siyu Lv, and Jizhong Chen. "Determination of the Optimum Heat Transfer Coefficient and Temperature Rise Analysis for a Lithium-Ion Battery under the Conditions of Harbin City Bus Driving Cycles". eng. In: *Energies (Basel)* 10.11 (2017), p. 1723. ISSN: 1996-1073.

[10] Peter Keil, Katharina Rumpf, and Andreas Jossen. “Thermal Impedance Spectroscopy for Li-Ion Batteries with an IR Temperature Sensor System”. In: *World Electric Vehicle Journal* 6 (Sept. 2013), pp. 581–591. DOI: 10.3390/wevj6030581.

[11] Ali Amini et al. “A thermal model for Li-ion batteries operating under dynamic conditions”. eng. In: *Applied thermal engineering* 185 (2021), p. 1. ISSN: 1359-4311.

[12] Inc. © 1994-2022 The MathWorks. *LSQnonlin Documentation*. 1999. URL: https://it.mathworks.com/help/optim/ug/lsqnonlin.html (visited on 06/13/2022).

[13] Inc. © 1994-2022 The MathWorks. *Equation Solving Algorithms Documentation*. 1999. URL: https://it.mathworks.com/help/optim/ug/equation-solving-algorithms.html (visited on 06/13/2022).

[14] Lichuan Wei et al. “A comprehensive study on thermal conductivity of the lithium-ion battery”. eng. In: *International journal of energy research* 44.12 (2020), pp. 9466–9478. ISSN: 0363-907X.